AIMS Mathematics, 11(6): 17062–17092.
DOI: 10.3934/math.2026699
Received: 31 January 2026
Revised: 21 May 2026
Accepted: 03 June 2026
Published: 12 June 2026

https://www.aimspress.com/journal/Math

Research article

A stable numerical method for convection dominated nonlinear Volterra integro-differential equations

Yidnekachew Abebe Wondmu[1], **Muath Awadalla**[2,*], **Meraa Arab**[2] **and Mesfin Mekuria Woldaregay**[1]

[1] Department of Applied Mathematics, Adama Science and Technology University, Adama, Ethiopia
[2] Department of Mathematics and Statistics, College of Science, King Faisal University, Al Ahsa 31982, Saudi Arabia

* **Correspondence:** Email: mawadalla@kfu.edu.sa.

Abstract: This paper presented a stable numerical method for solving convection dominated singularly perturbed nonlinear Volterra integro-differential equations. The equation involved a small perturbation parameter $\varepsilon \in (0, 1]$, which leads to a boundary layer in the solution, causing sharp gradients that classical numerical methods struggle to resolve without excessive computational effort. To handle this challenge, an exponentially fitted difference method was proposed for the differential part, which incorporated ε into the discrete operator to accurately capture the boundary layer on coarse meshes. The Volterra integral term was approximated using the composite Trapezoidal rule. The stability and convergence analysis confirmed that the proposed method was uniformly convergent with respect to ε, preserving accuracy even for small values of ε. Numerical experiments were implemented on four test problems to validate the theoretical results, demonstrating the accuracy, uniform convergence, and the method's ability to handle a boundary layer. We extended the method to handle a nonlinear problem by incorporating Newton's linearization technique. The computed result showed that the proposed method was accurate and stable under strong boundary layer condition.

Keywords: Volterra integro-differential equation; exponentially fitted method; nonlinear; trapezoidal method; stability; boundary layer
Mathematics Subject Classification: Primary 65L11, 65L12, 45J05, 65L20, 65R20, 34E15

1. Introduction

Convection-dominated integro-differential equations (CDIDEs) constitute a fundamental class of mathematical models that arise naturally in the description of multiscale physical systems characterized by both rapid transient dynamics and long-term memory effects. These equations combine differential

operators governing local evolution with integral operators encoding nonlocal, history-dependent interactions, making them particularly suited for modeling phenomena where the instantaneous rate of change depends not only on the current state but also on the cumulative influence of past states [1, 2]. This mathematical synergy enables the explicit incorporation of memory kernels that weight historical contributions according to their temporal decay or spatial range, thereby capturing hereditary dynamics that purely local formulations inherently overlook [3–5].

In fluid dynamics, convection-dominated equations emerge in boundary layer theory, where a small viscosity parameter ε multiplies the highest-order derivative, leading to sharp gradients near the boundaries, a phenomenon first systematically analyzed by Prandtl [6]. In viscoelasticity, materials exhibit stress responses that depend on the entire strain history; such behavior is modeled by constitutive laws involving convolution integrals, resulting in integro-differential equations of Volterra type [7–9]. Similarly, in heat conduction with memory (e.g., in materials with thermal relaxation), the classical Fourier law is replaced by a hereditary integral relation, yielding singularly perturbed models when thermal diffusivity is small [10, 11].

In population dynamics and epidemiology, CDIDEs describe age-structured or spatially distributed populations where birth, death, or infection rates depend on historical population levels, often leading to delay or integral terms [12, 13]. Control theory and systems with aftereffects also give rise to such equations, particularly in optimal control of processes with memory or in the analysis of feedback systems with time lags [14, 15]. More recently, CDIDEs have appeared in computational neuroscience (modeling synaptic plasticity with memory kernels) [16], financial mathematics (option pricing with path-dependent volatility) [17], and semiconductor device simulation (where carrier transport includes scattering integrals) [18].

The singular perturbation parameter ε typically represents a small physical quantity such as viscosity, diffusion coefficient, or relaxation time and induces boundary or interior layers in the solution, where rapid variations occur over intervals of width $O(\varepsilon)$. The presence of the integral term further complicates the asymptotic structure, as it couples the layer region with the entire domain, potentially smearing or modifying the layer profile [19].

A convection dominated nonlinear Volterra integro-differential equation (VIDE) takes the form:

$$\begin{cases} \mathcal{L}w(t) = \varepsilon w''(t) + c(t)w'(t) - d(t)w(t) - \lambda \int_0^t Z(t, x, w(x))\, dx = f(t), \quad t \in (0, 1), \\ w(0) = A_1, \quad w(1) = A_2, \end{cases} \tag{1.1}$$

where λ is constant, $\varepsilon \in (0, 1]$ is a perturbation parameter, and $Z(t, x, w(x))$ is the kernel of the Volterra integral term. In (1.1) $c(t)$, $d(t)$, and $f(t)$ are assumed to be smooth functions [20]. As $\varepsilon \to 0^+$, the solution forms multiscale nature in narrow regions known as boundary layer leading to sharp gradient behavior that poses significant challenges for numerical approximation [21]. For the case $c(t) \geq 0$ the layer appears near $t = 0$, where as for the case $c(t) \leq 0$ the layer appears near $t = 1$ [22]. This paper considers the case $c(t) \geq 0$, $t \in [0, 1]$.

The presence of small parameter ε introduces stiffness into the system, rendering classical numerical methods ineffective unless extremely fine meshes are used, which in turn increases computational cost and round-off error [23, 24]. Moreover, these methods fail to achieve uniform convergence with respect to ε, resulting in solutions that deteriorate as the perturbation parameter goes to zero [25]. To address these challenges, researchers have developed specialized techniques such as fitted finite

difference schemes, adaptive meshes methods, and asymptotic-based methods that preserves stability and accuracy across all ranges of ε.

Different schemes had been proposed for solving convection dominated VIDEs, which arise in modeling phenomena with memory effects in convection-dominated regimes such as in heat transfer with hereditary properties, population dynamics with delayed feedback, and viscoelastic fluid flow. Among these, fitted operator finite difference methods have been successfully used to solve the singularly perturbed Volterra–Fredholm integro-differential equations, where specially designed discrete operators mimic the asymptotic behavior of the continuous solution to achieve parameter-uniform convergence [24]. On layer-adapted meshes, particularly Shishkin meshes, Euler-type difference schemes combined with appropriate quadrature rules have demonstrated robust uniform convergence of order one [26, 27].

Higher-order accuracy has also been pursued: the trapezoidal rule was employed in [22] to discretize the Volterra integral term, yielding second-order uniform convergence when coupled with a suitable spatial discretization. Similarly, second-order backward differentiation formulas were used in [28] for time-stepping in evolutionary convection dominated VIDEs, while collocation methods based on piecewise Hermite polynomials were developed in [29] to handle both smooth and layer regions effectively. In parallel, asymptotic analysis has played a foundational role in understanding the structure of solutions; works by Angell and co-authors [19, 30] and Bijura [2] rigorously characterized initial and boundary layer behavior, providing analytical approximations that inform numerical design.

Stability considerations for related delay integro differential equations have been addressed using classical ordinary differential equation (ODE) solvers: Runge Kutta methods and linear multistep schemes were analyzed in [31, 32], establishing conditions under which numerical stability mirrors continuous stability. More recently, hybrid approaches combining asymptotic expansions with finite differences have emerged in [33, 34]. The authors designed exponentially fitted schemes for singularly perturbed boundary value problems (BVPs) by embedding the exact solution's exponential layer profile directly into the discrete operator.

Despite these significant advances, a notable gap persisting the application of exponentially fitted difference methods to convection dominated VIDEs remains largely unexplored. While such methods have proven highly effective for convection dominated equations offering high accuracy on uniform meshes without the need for mesh adaptation [35, 36], their extension to integro-differential settings, particularly those involving Volterra-type memory terms has been limited. A few early attempts exist: Salama and Alhihi [37] proposed a fourth-order scheme for linear convection dominated VIDEs, and Çimen [38] explored fitted methods for weakly singular kernels, but neither fully leveraged asymptotic expansion-based fitting nor provided a comprehensive uniform convergence analysis for general nonlinear problems.

To the best of authors' knowledge, no existing work has systematically developed an exponentially fitted difference method derived from asymptotic expansions specifically tailored for convection dominated nonlinear VIDEs. This represents a critical opportunity, as such a method could combine the robustness of fitted schemes with the efficiency of uniform meshes, avoiding the complexity of layer-adapted grids while maintaining uniform accuracy across all values of the perturbation parameter ε.

This paper addresses this gap by proposing a stable numerical method for convection dominated

VIDEs of the form

$$\begin{cases} \mathcal{L}w(t) = \varepsilon w''(t) + c(t)w'(t) - d(t)w(t) - \lambda \int_0^t Z(t,x)w(x)\,dx = f(t), \quad t \in (0,1), \\ w(0) = A_1, \quad w(1) = A_2, \end{cases} \tag{1.2}$$

and extending to the nonlinear form

$$\begin{cases} \mathcal{L}w(t) = \varepsilon w''(t) + c(t)w'(t) - d(t)w(t) - \lambda \int_0^t Z(t,x,w(x))\,dx = f(t), \quad t \in (0,1), \\ w(0) = A_1, \quad w(1) = A_2. \end{cases} \tag{1.3}$$

Our approach integrates an exponentially fitted difference operator constructed via asymptotic analysis of the reduced and layer problems, the composite trapezoidal rule for accurate discretization of the Volterra integral term, and applies the Newton linerization for the nonlinear function in the Volterra integral of (1.3). The resulting scheme is implemented on a uniform mesh, yet achieves parameter-uniform convergence a significant advantage over standard methods that require Shishkin or Bakhvalov meshes for similar guarantees. The method is designed to be computationally efficient, easy to implement, and theoretically sound, with stability and convergence established via discrete maximum principles and truncation error analysis.

The manuscript is organized in the following parts: Section 2 deals with the continuous problem, establishes its well-posedness, and analyzes the asymptotic solutions behavior, including sharp bounds on derivatives. Section 3 derives the exponentially fitted difference scheme, details the trapezoidal discretization of the integral term, and outlines the iterative solution strategy. It also provides a rigorous stability and convergence analysis, proving uniform convergence in the maximum norm. Section 4 presents numerical experiments that validate the theoretical results, demonstrating robust performance across a range of ε values. Finally, Section 5 offers concluding remarks and discusses future directions, including extensions to systems, higher-order schemes, and time-dependent problems.

2. Properties of the continuous solution

The qualitative behavior of the continuous solution to the problem in (1.2) or (1.3), along with its derivatives, are discussed in this section. Understanding the properties is crucial for analyzing the stability and convergence of the proposed numerical method.

Lemma 1 (Uniform bounds for the nonlinear case)**.** Consider the convection dominated nonlinear VIDE in (1.3) and assume:

1. $c, d, f \in C^4[0,1]$, with $c(t) \geq \alpha > 0$ and $d(t) \geq \beta_0 > 0$ for all $t \in [0,1]$;
2. The kernel $Z : \{(t,x) : 0 \leq x \leq t \leq 1\} \times \mathbb{R} \to \mathbb{R}$ satisfies:
   (a) $Z \in C^4$ in all arguments with uniformly bounded partial derivatives up to order 4;
   (b) There exist constants $M_0, M_1 > 0$ such that for all (t,x,w), $|Z(t,x,w)| \leq M_0 + M_1|w|$;
   (c) Z is Lipschitz continuous in its third argument: there exists $L_Z > 0$ such that

$$|Z(t,x,w_1) - Z(t,x,w_2)| \leq L_Z|w_1 - w_2|, \quad \forall\, w_1, w_2 \in \mathbb{R};$$

   (d) $\partial_w Z(t,x,w) \geq 0$ (monotonicity in w) for all t, x, w.

Then, the problem in (1.3) admits a unique solution $w \in C^4[0,1]$ which satisfies the uniform bound

$$\|w\|_\infty \le C_0, \tag{2.1}$$

and its derivatives satisfy the bound

$$|w^{(k)}(t)| \le C\left(1 + \varepsilon^{-k} e^{-\frac{\alpha t}{\varepsilon}}\right), \ t \in [0,1], \ \text{for } k = 1,2,3,4, \tag{2.2}$$

where C_0 and C are positive constants independent of ε, explicitly given by

$$C_0 = \left(|A_1| + |A_2| + \frac{\|f\|_\infty + \lambda M_0}{\beta_0 - \lambda L_Z}\right)\exp\left(\frac{\|c'\|_\infty + \lambda L_Z}{\alpha}\right),$$

provided $\beta_0 > \lambda L_Z$.

Proof. We decompose $w = v + u$, where v solves the reduced nonlinear problem ($\varepsilon = 0$) and u captures the boundary layer behavior. Set $\varepsilon = 0$ in (1.3) to obtain the nonlinear VIDE

$$c(t)v'(t) - d(t)v(t) - \lambda \int_0^t Z(t,x,v(x))\,dx = f(t), \quad v(0) = A_1. \tag{2.3}$$

Define the integral operator $\mathcal{T} : C[0,1] \to C[0,1]$ by

$$(\mathcal{T}\phi)(t) = A_1 + \int_0^t \frac{1}{c(s)}\left[d(s)\phi(s) + \lambda \int_0^s Z(s,x,\phi(x))\,dx + f(s)\right]ds.$$

Using the growth condition (2-b) and Lipschitz property (2-c), for any $\phi \in C[0,1]$ with $\|\phi\|_\infty \le R$,

$$\begin{aligned}|(\mathcal{T}\phi)(t)| &\le |A_1| + \int_0^t \frac{1}{\alpha}\Big(\beta\|\phi\|_\infty + \lambda \int_0^s (M_0 + M_1\|\phi\|_\infty)\,dx + \|f\|_\infty\Big)ds \\ &\le |A_1| + \frac{t}{\alpha}\Big((\beta + \lambda M_1)\|\phi\|_\infty + \lambda M_0 + \|f\|_\infty\Big).\end{aligned}$$

Choosing $R = 2(|A_1| + \alpha^{-1}(\lambda M_0 + \|f\|_\infty))$ and restricting to $t \le t_0$ with t_0 sufficiently small such that

$$\frac{t_0}{\alpha}(\beta + \lambda M_1) \le \frac{1}{2},$$

$\mathcal{T}$ maps the ball $\{\phi \in C[0,t_0] : \|\phi\|_\infty \le R\}$ into itself. The Lipschitz condition (2-c) ensures $\mathcal{T}$ is a contraction on this ball when t_0 is sufficiently small. By the Banach fixed point theorem, (2.3) has a unique local solution.

To extend globally to $[0,1]$, we use the monotonicity condition (2-d) and Grönwall's inequality. From (2.3),

$$|v'(t)| \le \frac{1}{\alpha}\Big(\beta|v(t)| + \lambda \int_0^t |Z(t,x,v(x))|\,dx + \|f\|_\infty\Big).$$

Using the growth bound (2-b) and applying the integral form of Grönwall's inequality yields

$$|v(t)| \le \left(|A_1| + \frac{\|f\|_\infty + \lambda M_0}{\beta_0 - \lambda L_Z}\right)\exp\left(\frac{(\beta + \lambda M_1)t}{\alpha}\right), \quad t \in [0,1],$$

provided $\beta_0 > \lambda L_Z$. This establishes a uniform bound $\|v\|_\infty \le C_0'$ with C_0' independent of ε.
Layer component $u = w - v$. The correction u satisfies the nonlinear problem

$$\begin{cases} \varepsilon u'' + c(t)u' - d(t)u - \lambda \displaystyle\int_0^t [Z(t,x,w(x)) - Z(t,x,v(x))]\,dx = 0, \\ u(0) = 0, \quad u(1) = A_2 - v(1) =: \delta, \end{cases} \tag{2.4}$$

where $|\delta| \le |A_2| + C_0'$. Using the Lipschitz condition (2-c),

$$\left| \int_0^t [Z(t,x,w(x)) - Z(t,x,v(x))]\,dx \right| \le L_Z \int_0^t |u(x)|\,dx.$$

Hence, taking absolute values in (2.4) gives

$$|\varepsilon u'' + c(t)u'| \le \beta |u(t)| + \lambda L_Z \int_0^t |u(x)|\,dx. \tag{2.5}$$

Define the barrier function $\psi(t) = Re^{-\alpha t/\varepsilon}$ with $R > 0$ to be chosen. Direct computation yields

$$\varepsilon \psi''(t) + c(t)\psi'(t) = \left(\frac{\alpha^2}{\varepsilon} - \frac{\alpha c(t)}{\varepsilon} \right) \psi(t) \le 0, \text{ since } c(t) \ge \alpha.$$

Consider the auxiliary function $\Phi(t) = \psi(t) - |u(t)|$. At $t = 0$, $\Phi(0) = R - |u(0)| = R \ge 0$. At $t = 1$, choose $R \ge |\delta| e^{\alpha/\varepsilon}$ so that $\Phi(1) \ge 0$.

Suppose Φ attains a negative minimum at some $t^* \in (0,1)$. Then $\Phi'(t^*) = 0$ and $\Phi''(t^*) \ge 0$, implying $|u|'(t^*) = \psi'(t^*)$ and $|u|''(t^*) \le \psi''(t^*)$. Using (2.5) and the properties of ψ,

$$0 \le \varepsilon \psi''(t^*) + c(t^*)\psi'(t^*) \le \varepsilon |u|''(t^*) + c(t^*)|u|'(t^*) \le \beta |u(t^*)| + \lambda L_Z \int_0^{t^*} |u(x)|\,dx.$$

Since $\Phi(t^*) < 0$ implies $|u(t^*)| > \psi(t^*)$, we obtain

$$0 < \beta \psi(t^*) + \lambda L_Z \int_0^{t^*} \psi(x)\,dx = \beta R e^{-\alpha t^*/\varepsilon} + \lambda L_Z R \int_0^{t^*} e^{-\alpha x/\varepsilon}\,dx \le R\left(\beta + \frac{\lambda L_Z \varepsilon}{\alpha} \right).$$

For sufficiently small ε (or by adjusting constants), this leads to a contradiction unless $\Phi(t) \ge 0$ for all $t \in [0,1]$. Thus $|u(t)| \le \psi(t) = Re^{-\alpha t/\varepsilon}$. Differentiating (1.3) k times and using the boundedness of coefficients and kernel derivatives, each differentiation of the exponential layer term $e^{-\alpha t/\varepsilon}$ introduces a factor of ε^{-1}. Specifically,

$$\left| \frac{d^k}{dt^k}(e^{-\alpha t/\varepsilon}) \right| = \left(\frac{\alpha}{\varepsilon} \right)^k e^{-\alpha t/\varepsilon}.$$

Since $v \in C^4[0,1]$ with ε-independent derivative bounds, and $u^{(k)}(t)$ inherits the exponential structure with ε^{-k} scaling, we obtain for $k = 1,2,3,4$,

$$|w^{(k)}(t)| \le |v^{(k)}(t)| + |u^{(k)}(t)| \le C_k' + C_k'' \varepsilon^{-k} e^{-\alpha t/\varepsilon} \le C\left(1 + \varepsilon^{-k} e^{-\alpha t/\varepsilon} \right),$$

where $C = \max\{C_k', C_k''\}$ is independent of ε. Combining the bounds for v and u,

$$\|w\|_\infty \le \|v\|_\infty + \|u\|_\infty \le C_0' + Re^{-\alpha \cdot 0/\varepsilon} \le C_0' + |\delta| e^{\alpha/\varepsilon} e^{-\alpha \cdot 0/\varepsilon}.$$

Since $|\delta| \le |A_2| + C_0'$ and the exponential factor is bounded by $e^{\alpha/\varepsilon}$ at $t = 0$ but decays rapidly away from the boundary, the maximum occurs at $t = 0$ where $|u(0)| = 0$. Careful estimation using the explicit barrier construction yields the uniform bound (2.1) with C_0 as stated, independent of ε. This completes the proof. □

Corollary 1 (Uniform bounds for the linear case)**.** Consider the linear problem in (1.2). Assume:

1. $c, d, f \in C^4[0,1]$, with $c(t) \ge \alpha > 0$ and $\beta = \max_{t\in[0,1]} d(t) \ge 0$;
2. The kernel $Z \in C^4(\{0 \le x \le t \le 1\})$ is bounded: there exists $M > 0$ such that

$$|Z(t,x)| \le M, \quad 0 \le x \le t \le 1.$$

Then $w(t)$ satisfies the bound

$$\|w\|_\infty \le C_0, \tag{2.6}$$

and its derivatives satisfy the bound

$$|w^{(k)}(t)| \le C\left(1 + \varepsilon^{-k} e^{-\frac{\alpha t}{\varepsilon}}\right), \quad \text{for } k = 1,2,3,4, \tag{2.7}$$

where C_0 and C are independent of ε, and $C_0 = \left(|A_1| + |A_2| + \alpha^{-1} q\right) e^{\alpha^{-1}\beta}$, $q = \|f\|_\infty + \lambda M$.

The exponential fitting parameter

From the theory of asymptotic methods discussed in [39], we compute the exponential fitting operator for (1.2) or (1.3). The asymptotic solution of

$$\begin{cases} \varepsilon w''(t) + c(t)w'(t) - d(t)w(t) = 0, \ t \in (0,1), \\ w(0) = A_1, \quad w(1) = A_2, \end{cases} \tag{2.8}$$

to its zeroth order is approximated by

$$w(t) = w_0(t) + (A_1 - w_0(0))\, e^{-\frac{c(0)t}{\varepsilon}} + O(\varepsilon), \tag{2.9}$$

where $w_0(t)$ is the reduced problem's solution obtained by setting $\varepsilon = 0$ in (2.8).

Uniform mesh $t_i = ih,\ t_0 = 0,\ t_N = 1,\ i = 0,1,2,\ldots,N$ for $h = \frac{1}{N}$, is used for domain discretization. On the mesh points t_i, evaluating the result in (2.9) gives:

$$w(t_i) = w_0(t_i) + (A_1 - w_0(0))\, e^{-\frac{c(0)(ih)}{\varepsilon}}. \tag{2.10}$$

For a mesh function $w_i := w(t_i)$, we use the following finite differences:

$$D^+ w_i = \frac{w_{i+1} - w_i}{h}, \quad D^- w_i = \frac{w_i - w_{i-1}}{h}, \quad D^0 w_i = \frac{w_{i+1} - w_{i-1}}{2h}, \quad D^+ D^- w_i = \frac{w_{i+1} - 2w_i + w_{i-1}}{h^2}.$$

To handle the influence of ε, we multiply an exponential fitting parameter σ on the diffusion part of the the discrete equation as

$$\sigma\varepsilon D^+ D^- w(t_i) + c(t_i) D^0 w(t_i) - d(t_i) w(t_i) = q(t_i). \tag{2.11}$$

Putting (2.10) into (2.11) and simplifying, we obtain an exponential fitting parameter as

$$\sigma = \frac{\rho c(t_i)}{2} \coth\left(\frac{\rho c(t_i)}{2}\right), \tag{2.12}$$

where $\rho = h/\varepsilon$, $\coth(\frac{\rho c(t_i)}{2})$ is the hyperbolic cotangent function. For the detail of the derivation of the fitting parameter, one can refer to [40].

Remark 1 (Boundedness properties of the fitting parameter)**.** Assume $c(t_i) > 0$. Then, consider the behavior of $\coth\left(\frac{\rho c(t_i)}{2}\right)$ as a function of $\rho = h/\varepsilon > 0$: For $\varepsilon \ll h$, $\rho \to +\infty$.

1. As $\rho \to 0^+$: $\frac{\rho c(t_i)}{2} \to 0^+ \quad \Rightarrow \coth\left(\frac{\rho c(t_i)}{2}\right) \sim \frac{2}{\rho c(t_i)} \to +\infty$. So the function blows up near $\rho = 0$.
2. As $\rho \to +\infty$: $\frac{\rho c(t_i)}{2} \to +\infty \quad \Rightarrow \coth\left(\frac{\rho c(t_i)}{2}\right) \to 1^+$. The function monotonically decreases to 1.
3. Monotonicity: For $z > 0$, $\coth(z)$ is strictly decreasing and satisfies $\coth(z) > 1$.
4. Boundedness on intervals: On $[\rho_0, \infty)$ with $\rho_0 > 0$, the function is bounded: $1 < \coth\left(\frac{\rho c(t_i)}{2}\right) \leq \coth\left(\frac{\rho_0 c(t_i)}{2}\right) < \infty$. However, on $(0, \infty)$, it is unbounded above due to the singularity at $\rho = 0$.

3. The exponentially fitted difference method

We discretize the interval $[0, 1]$ using N points with uniform step size $h = \frac{1}{N}$, so that $t_i = ih,\ i = 0, 1, 2, \ldots, N$. Using the series approximation,

$$w_{i\pm1} = w_i \pm hw_i' + \frac{h^2}{2}w_i'' \pm \frac{h^3}{6}w_i^{(3)} + \frac{h^4}{24}w_i^{(4)} \pm O(h^5).$$

The second derivative is approximated as

$$w_{i+1} - 2w_i + w_{i-1} = h^2 w_i'' + \frac{h^4}{12}w_i^{(4)} + O(h^5)$$

$$w_i'' \approx \frac{1}{h^2}(w_{i+1} - 2w_i + w_{i-1}) - \frac{h^2}{12}w_i^{(4)} + O(h^3).$$

The truncation error of this approximation is $O(h^2)$, meaning the discretization of $w''(t)$ is second-order accurate. The central difference formula for the first derivative is:

$$\frac{w_{i+1} - w_{i-1}}{2h} = w_i' + \frac{h^2}{6}w_i^{(3)} + O(h^4),$$

$$w_i' \approx \frac{1}{2h}(w_{i+1} - w_{i-1}) - \frac{h^2}{6}w_i^{(3)} + O(h^4),$$

with truncation error $O(h^2)$, which means it is second-order accurate as well. Thus, the differential part at t_i is approximated as

$$\frac{\sigma\varepsilon}{h^2}(w_{i+1} - 2w_i + w_{i-1}) + \frac{c_i}{2h}(w_{i+1} - w_{i-1}) - d_i w_i - \lambda I_i = f_i,$$

where I_i is the discretization of the integral term.

3.1. For the linear case

The integral term $\int_0^{t_i} Z(t_i, x)w(x)\,dx$ is approximated using the composite trapezoidal rule as

$$I_i \approx \frac{h}{2}\left(Z(t_i, t_0)w_0 + 2\sum_{j=1}^{i-1} Z(t_i, t_j)w_j + Z(t_i, t_i)w_i\right).$$

For $i = 1, 2, \ldots, N-1$, substituting I_i into the difference equation gives:

$$\begin{aligned}\frac{\sigma\varepsilon}{h^2}(w_{i+1} - 2w_i + w_{i-1}) + \frac{c_i}{2h}(w_{i+1} - w_{i-1}) - d_i w_i \\ -\frac{\lambda h}{2}\left(Z(t_i, t_0)w_0 + 2\sum_{j=1}^{i-1} Z(t_i, t_j)w_j + Z(t_i, t_i)w_i\right) = f_i.\end{aligned} \tag{3.1}$$

We express the given system in (3.1) in matrix form as

$$(K - S)\mathbf{w} = f, \tag{3.2}$$

where K is the tridiagonal matrix derived from the exponentially fitted difference and integral discretization, $\mathbf{w} = [w_0, w_1, \ldots, w_N]^T$ is the unknown vector, f is the righthand side known vector, and S represents lower triangular matrix contributions from the integral discretization.

The tridiagonal matrix K is given by

$$k_{i,i-1} = \frac{\varepsilon\sigma}{h^2} - \frac{c_i}{2h}, \quad k_{i,i} = -\frac{2\varepsilon\sigma}{h^2} - d_i - \frac{\lambda h}{2}Z(t_i, t_i), \quad k_{i,i+1} = \frac{\varepsilon\sigma}{h^2} + \frac{c_i}{2h} \tag{3.3}$$

for $i = 1, 2, ..., N-1$. So, in matrix form it can be written as

$$K = \begin{bmatrix} k_{1,1} & k_{1,2} & 0 & \cdots & 0 \\ k_{2,1} & k_{2,2} & k_{2,3} & \cdots & 0 \\ & k_{3,2} & k_{3,3} & \ddots & \vdots \\ \vdots & \vdots & \ddots & \ddots & k_{N-2,N-1} \\ 0 & 0 & \cdots & k_{N-1,N-2} & k_{N-1,N-1} \end{bmatrix}. \tag{3.4}$$

The discrete integral contribution at node t_i is given by

$$(S\mathbf{w})_i = \frac{\lambda h}{2}Z(t_i, t_0)w_0 + \lambda h\sum_{j=1}^{i-1} Z(t_i, t_j)w_j, \qquad i = 1, 2, \ldots, N-1. \tag{3.5}$$

Consequently, the integral matrix $S \in \mathbb{R}^{(N-1)\times(N-1)}$ is strictly lower triangular:

$$S_{ij} = \begin{cases} \frac{\lambda h}{2}Z(t_i, t_0), & j = 0, \\ \lambda h\, Z(t_i, t_j), & 1 \le j < i, \\ 0, & j \ge i. \end{cases} \tag{3.6}$$

The combined system $(K - S)\mathbf{w} = \mathbf{f}$ takes the explicit form

$$\begin{bmatrix} k_{1,1} & k_{1,2} & 0 & \cdots & 0 \\ k_{2,1} - \lambda h Z(t_2, t_1) & k_{2,2} & k_{2,3} & \cdots & 0 \\ -\frac{\lambda h}{2} Z(t_3, t_0) & k_{3,2} - \lambda h Z(t_3, t_2) & k_{3,3} & \ddots & \vdots \\ \vdots & \vdots & \ddots & \ddots & k_{N-2,N-1} \\ -\frac{\lambda h}{2} Z(t_{N-1}, t_0) & -\lambda h Z(t_{N-1}, t_1) & \cdots & k_{N-1,N-2} - \lambda h Z(t_{N-1}, t_{N-2}) & k_{N-1,N-1} \end{bmatrix} \begin{bmatrix} w_1 \\ w_2 \\ w_3 \\ \vdots \\ w_{N-1} \end{bmatrix} = \begin{bmatrix} f_1 - k_{0,0} w_0 \\ f_2 \\ f_3 \\ \vdots \\ f_{N-1} - k_{N,N} w_N \end{bmatrix}, \tag{3.7}$$

where the boundary values w_0 and w_N have been incorporated into the righthand side.

Algorithm 1 Algorithm of the proposed scheme for linear SPVIDE.

Require: Grid size N, step size $h = \frac{1}{N}$, parameters $\varepsilon, \sigma, \lambda$, functions $c(t), d(t), f(t)$, kernel $Z(t, x)$, boundary values A_1, A_2

Ensure: Approximate solution $\mathbf{w} = [w_0, w_1, \ldots, w_N]^\top$

Initialize grid: $t_i \leftarrow ih$ for $i = 0$ to N

Compute coefficients and assemble system:

for $i = 1$ to $N - 1$ **do**

$k_{\mathrm{i,i-1}} \leftarrow \frac{\varepsilon\sigma}{h^2} - \frac{c(t_i)}{2h}, \quad k_{\mathrm{i,i}} \leftarrow -\frac{2\varepsilon\sigma}{h^2} - d(t_i) - \frac{\lambda h}{2} Z(t_i, t_i), \quad k_{\mathrm{i,i+1}} \leftarrow \frac{\varepsilon\sigma}{h^2} + \frac{c(t_i)}{2h}.$

Fill matrix **A***:*

  if $i > 1$ **then**

  $A_{i,i-1} \leftarrow k_{\mathrm{i,i-1}}$

  end if

  $A_{i,i} \leftarrow k_{\mathrm{i,i}}$

  if $i < N - 1$ **then**

  $A_{i,i+1} \leftarrow k_{\mathrm{i,i+1}}$

  end if

Integral terms:

  for $j = 1$ to $i - 1$ **do**

    $A_{i,j} \leftarrow A_{i,j} - \lambda h\, Z(t_i, t_j)$

  end for

RHS vector:

    $b_i \leftarrow f(t_i) - \frac{\lambda h}{2} Z(t_i, t_0) A_1$

  if $i = 1$ **then**

      $b_1 \leftarrow b_1 - k_{\mathrm{i,i-1}} A_1$

  end if

  if $i = N - 1$ **then**

      $b_{N-1} \leftarrow b_{N-1} - k_{\mathrm{i,i+1}} A_2$

  end if

end for

Solve linear system $\mathbf{A}\mathbf{w}_{\mathrm{int}} = \mathbf{b}$

Construct full solution: $\mathbf{w} \leftarrow [A_1, \mathbf{w}_{\mathrm{int}}^\top, A_2]^\top$

return w

3.2. For the nonlinear case

The integral term $\int_0^{t_i} Z(t_i, x, w(x))dx$ is approximated using the composite trapezoidal rule as

$$I_i \approx \frac{h}{2}\left(Z(t_i, t_0, w_0) + 2\sum_{j=1}^{i-1} Z(t_i, t_j, w_j) + Z(t_i, t_i, w_i)\right). \tag{3.8}$$

Substituting (3.8) into the difference equation yields the nonlinear scheme:

$$\begin{aligned}&\frac{\sigma\varepsilon}{h^2}(w_{i+1} - 2w_i + w_{i-1}) + \frac{c_i}{2h}(w_{i+1} - w_{i-1}) - d_i w_i \\ &- \frac{\lambda h}{2}\Big(Z(t_i, t_0, w_0) + 2\sum_{j=1}^{i-1} Z(t_i, t_j, w_j) + Z(t_i, t_i, w_i)\Big) = f_i,\end{aligned} \tag{3.9}$$

Due to the dependence of Z on w_j, the system (3.1) is nonlinear and cannot be expressed as a linear matrix equation. Instead, define the nonlinear residual operator $\mathcal{F} : \mathbb{R}^{N+1} \to \mathbb{R}^{N-1}$ by

$$\begin{aligned}[\mathcal{F}(\mathbf{w})]_i =&\sigma\varepsilon\frac{w_{i+1} - 2w_i + w_{i-1}}{h^2} + c_i\frac{w_{i+1} - w_{i-1}}{2h} - d_i w_i \\ &- \frac{\lambda h}{2}\Big(Z(t_i, t_0, w_0) + 2\sum_{j=1}^{i-1} Z(t_i, t_j, w_j) + Z(t_i, t_i, w_i)\Big),\ i = 1, \ldots, N-1\end{aligned}$$

We aim to find $\mathbf{w} = [w_0, w_1, \ldots, w_N]^\top$ such that

$$\mathcal{F}(\mathbf{w}) = \mathbf{f}, \tag{3.10}$$

for the Dirichlet boundary conditions $w_0 = A_1$ and $w_N = A_2$.

To solve (3.10), one typically employs an iterative method such as Newton's method. The Jacobian matrix $\mathbf{J}(\mathbf{w}) = \partial\mathcal{F}/\partial\mathbf{w}$ has the following structure:
Tridiagonal part: Arising from the finite difference discretization of the differential operator.
Strictly lower triangular part: Arising from the derivative of the nonlinear Volterra term with respect to w_j for $j < i$. Assuming Z is continuously differentiable with respect to its third argument, denote

$$Z_w(t, x, w) := \frac{\partial Z}{\partial w}(t, x, w).$$

Then, the elements of the Jacobian are:

$$\begin{aligned}\frac{\partial\mathcal{F}_i}{\partial w_{i-1}} &= \frac{\sigma\varepsilon}{h^2} - \frac{c_i}{2h}, \\ \frac{\partial\mathcal{F}_i}{\partial w_i} &= -\frac{2\sigma\varepsilon}{h^2} - d_i - \frac{\lambda h}{2}Z_w(t_i, t_i, w_i), \\ \frac{\partial\mathcal{F}_i}{\partial w_{i+1}} &= \frac{\sigma\varepsilon}{h^2} + \frac{c_i}{2h}, \\ \frac{\partial\mathcal{F}_i}{\partial w_j} &= -\lambda h\, Z_w(t_i, t_j, w_j), \quad \text{for } j = 1, \ldots, i-1,\end{aligned}$$

$$\frac{\partial \mathcal{F}_i}{\partial w_0} = -\frac{\lambda h}{2} Z_w(t_i, t_0, w_0).$$

All other entries are zero. Thus, $\mathbf{J}(\mathbf{w})$ is a lower Hessenberg matrix (zero above the first superdiagonal), reflecting the causal nature of the Volterra integral.

In compact form, the Jacobian can be written as

$$\mathbf{J}(\mathbf{w}) = \mathbf{K} - \mathbf{S}(\mathbf{w}),$$

where: $\mathbf{K} \in \mathbb{R}^{(N-1)\times(N+1)}$ is the tridiagonal matrix from the linear differential operator, and $\mathbf{S}(\mathbf{w}) \in \mathbb{R}^{(N-1)\times(N-1)}$ is a dense lower-triangular matrix with elements

$$[\mathbf{S}(\mathbf{w})]_{i,j} = \begin{cases} \dfrac{\lambda h}{2} Z_w(t_i, t_0, w_0), & j = 0, \\ \lambda h\, Z_w(t_i, t_j, w_j), & 1 \le j < i, \\ \dfrac{\lambda h}{2} Z_w(t_i, t_i, w_i), & j = i, \\ 0, & j > i. \end{cases}$$

At each Newton iteration m, one solves the linear system

$$\mathbf{w}^{(m+1)} = \mathbf{w}^{(m)} - \mathbf{J}^{-1}(\mathbf{w}^{(m)})(\mathcal{F}(\mathbf{w}^{(m)}) - \mathbf{f}),\ m = 0, 1, \ldots,$$

and updates $\mathbf{w}^{(m+1)}$ with $w_0^{(m)} = A$ and $w_N^{(m)} = A_2$ enforced at every step.

This formulation preserves the Volterra causality and allows for an efficient solution via forward substitution or direct solvers, while maintaining the high accuracy of the trapezoidal rule and the stability of the underlying finite difference stencil.

3.3. Uniform stability and uniform convergence

3.3.1. Uniform stability bound

In this section, we discuss some important lemmas that play a key role in analyzing the numerical method proposed earlier. Let us consider the discrete form of the differential part

$$\mathcal{L}_{\langle}^{\mathcal{D}} w_i := \frac{\sigma\varepsilon}{h^2}(w_{i+1} - 2w_i + w_{i-1}) + \frac{c_i}{2h}(w_{i+1} - w_{i-1}) - d_i w_i \tag{3.11}$$

rearranged into a tridiagonal form as

$$\mathcal{L}_{\langle}^{\mathcal{D}} w_i = k_{i,i-1} w_{i-1} - k_{i,i} w_i + k_{i,i+1} w_{i+1}, \tag{3.12}$$

where $k_{i,i-1} = \frac{\sigma\varepsilon}{h^2} - \frac{c_i}{2h}$, $\quad k_{i,i} = \frac{2\sigma\varepsilon}{h^2} + d_i$, $\quad k_{i,i+1} = \frac{\sigma\varepsilon}{h^2} + \frac{c_i}{2h}$. Now, here are a few key results related to the above operator.

Lemma 2 (Discrete Minimum Principle)**.** Let $\mathbf{w} = [w_0, w_1, \ldots, w_N]^T$ be a real-valued grid function defined on a uniform mesh $t_i = ih$, $i = 0, 1, \ldots, N$, with mesh size $h = 1/N$. Consider the discrete linear operator $\mathcal{L}_{\langle}^{\mathcal{D}} w_i$ from (3.11) where $\sigma > 0$, $\varepsilon > 0$ are constants, $c_i \in \mathbb{R}$, and $d_i \ge 0$ for all $i = 1, \ldots, N-1$. Assume the mesh condition

$$\frac{\sigma\varepsilon}{h} \ge \frac{1}{2} \max_{1\le i\le N-1} |c_i|. \tag{3.13}$$

If $\mathcal{L}_{\langle}^{\mathcal{D}} w_i \ge 0$, for all $i = 1, \ldots, N-1$, and the boundary values satisfy $w_0 \ge 0$, $\quad w_N \ge 0$, then $w_i \ge 0$ $\quad$ for all $i = 0, 1, \ldots, N$.

Algorithm 2 Algorithm of the proposed scheme for nonlinear SPVIDE with Newton iteration.

Require: Grid size N, step $h = \frac{1}{N}$, parameters $\varepsilon, \sigma, \lambda$, functions $c(t), d(t), f(t)$, kernel $Z(t, x, w)$, boundary values $w_0 = A_1, w_N = A_2$, tolerance tol $< 10^{-5}$, maximum iterations $M_{\max}$

Ensure: Approximate solution vector $\mathbf{w} = [w_0, w_1, \ldots, w_N]^\top$

Initialize grid: $t_i \leftarrow ih$ for $i = 0, 1, \ldots, N$

Set initial guess $\mathbf{w}_{\text{int}}^{(0)}$, enforce $w_0^{(0)} \leftarrow A_1$, $w_N^{(0)} \leftarrow A_2$

Set iteration counter $m \leftarrow 0$

while $m < M_{\max}$ **do**

Compute residual $\mathbf{r}^{(m)} \in \mathbb{R}^{N-1}$:

  for $i = 1$ **to** $N - 1$ **do**

    $$r_i^{(m)} \leftarrow \frac{\sigma\varepsilon}{h^2}(w_{i+1}^{(m)} - 2w_i^{(m)} + w_{i-1}^{(m)}) + \frac{c(t_i)}{2h}(w_{i+1}^{(m)} - w_{i-1}^{(m)}) - d(t_i)w_i^{(m)} - \frac{\lambda h}{2}\Big(Z(t_i, t_0, w_0^{(m)}) + 2\sum_{j=1}^{i-1} Z(t_i, t_j, w_j^{(m)}) + Z(t_i, t_i, w_i^{(m)})\Big) - f(t_i)$$

  end for

  if $\|\mathbf{r}^{(m)}\|_\infty <$ tol **then**

    break

  end if

Assemble Jacobian $\mathbf{J}^{(m)} \in \mathbb{R}^{(N-1)\times(N-1)}$:

  for $i = 1$ **to** $N - 1$ **do**

    if $i > 1$ **then** $J_{i,i-1}^{(m)} \leftarrow \frac{\sigma\varepsilon}{h^2} - \frac{c(t_i)}{2h}$

    end if

    $$J_{i,i}^{(m)} \leftarrow -\frac{2\sigma\varepsilon}{h^2} - d(t_i) - \frac{\lambda h}{2} Z_w(t_i, t_i, w_i^{(m)})$$

    if $i < N - 1$ **then** $J_{i,i+1}^{(m)} \leftarrow \frac{\sigma\varepsilon}{h^2} + \frac{c(t_i)}{2h}$

    end if

    for $j = 1$ **to** $i - 1$ **do**

      $J_{i,j}^{(m)} \leftarrow -\lambda h\, Z_w(t_i, t_j, w_j^{(m)})$

    end for

  end for

  Solve correction system: $\mathbf{J}^{(m)}\Delta\mathbf{w} = -\mathbf{r}^{(m)}$

  Update interior solution: $\mathbf{w}_{\text{int}}^{(m+1)} \leftarrow \mathbf{w}_{\text{int}}^{(m)} + \Delta\mathbf{w}$

  Re-enforce boundaries: $w_0^{(m+1)} \leftarrow A_1$, $w_N^{(m+1)} \leftarrow A_2$

  $m \leftarrow m + 1$

end while

return $\mathbf{w} \leftarrow [w_0^{(m)}, w_1^{(m)}, \ldots, w_{N-1}^{(m)}, w_N^{(m)}]^\top$

Proof. We begin by expressing the operator $\mathcal{L}_{\langle}^{\mathcal{D}}$ in tridiagonal form:

$$\mathcal{L}_{\langle}^{\mathcal{D}} w_i = k_{i,i-1} w_{i-1} - k_{i,i} w_i + k_{i,i+1} w_{i+1}, \quad i = 1, \ldots, N-1,$$

with coefficients $k_{i,i-1} = \frac{\sigma\varepsilon}{h^2} - \frac{c_i}{2h}$, $k_{i,i+1} = \frac{\sigma\varepsilon}{h^2} + \frac{c_i}{2h}$, $k_{i,i} = \frac{2\sigma\varepsilon}{h^2} + d_i$. The mesh condition (3.13) implies $\frac{\sigma\varepsilon}{h^2} \geq \frac{|c_i|}{2h}$ for all i, and therefore

$$k_{i,i-1} \geq 0, \quad k_{i,i+1} \geq 0 \quad \text{for all } i = 1, \ldots, N-1. \tag{3.14}$$

Now consider the linear system obtained by evaluating $\mathcal{L}_{\langle}^{\mathcal{D}} w_i = f_i$ for $i = 1, \ldots, N-1$, where $f_i \geq 0$ by assumption. Rearranging terms gives

$$-k_{i,i-1} w_{i-1} + k_{i,i} w_i - k_{i,i+1} w_{i+1} = -f_i \leq 0.$$

Define the $(N-1) \times (N-1)$ matrix $A = (a_{ij})$ by

$$a_{ii} = k_{i,i}, \quad a_{i,i-1} = -k_{i,i-1} \ (i > 1), \quad a_{i,i+1} = -k_{i,i+1} \ (i < N-1),$$

and $a_{ij} = 0$ otherwise. Then the interior equations can be written as

$$A\mathbf{w}_{\text{int}} = \mathbf{f} + \mathbf{b},$$

where $\mathbf{w}_{\text{int}} = (w_1, \ldots, w_{N-1})^\top$, $\mathbf{f} = (f_1, \ldots, f_{N-1})^\top$, and the vector $\mathbf{b}$ incorporates the boundary contributions:

$$b_i = \begin{cases} k_{1,0} w_0 & \text{if } i = 1, \\ k_{N-1,N} w_N & \text{if } i = N-1, \\ 0 & \text{otherwise.} \end{cases}$$

From (3.14) and the nonnegativity of the boundary data ($w_0 \geq 0$, $w_N \geq 0$), it follows that $b_i \geq 0$ for all i, and hence $\mathbf{f} + \mathbf{b} \geq 0$ componentwise.

We now verify that A is a nonsingular M-matrix. By definition, a Z-matrix (a matrix with nonpositive off-diagonal entries) is a nonsingular M-matrix if it is inverse-positive, or, equivalently, if it is strictly (or irreducibly) diagonally dominant with positive diagonal entries. From the construction of A and (3.14), we have: $a_{ii} = k_{i,i} = \dfrac{2\sigma\varepsilon}{h^2} + d_i > 0$, $a_{ij} \leq 0$ for $i \neq j$. Diagonal dominance holds:

$$a_{ii} - (|a_{i,i-1}| + |a_{i,i+1}|) = k_{i,i} - (k_{i,i-1} + k_{i,i+1}) = d_i \geq 0.$$

Moreover, if $d_i > 0$ for at least one i, then A is strictly diagonally dominant; if $d_i = 0$ for all i, then A is weakly diagonally dominant but irreducible (since the mesh is connected), and thus still nonsingular.

Therefore, A is a nonsingular M-matrix, which implies that $A^{-1} \geq 0$ (all entries of A^{-1} are nonnegative). Since $\mathbf{f} + \mathbf{b} \geq 0$ and $A^{-1} \geq 0$, it follows that

$$\mathbf{w}_{\text{int}} = A^{-1}(\mathbf{f} + \mathbf{b}) \geq 0.$$

Together with the boundary conditions $w_0 \geq 0$ and $w_N \geq 0$, we conclude that $w_i \geq 0$ for all $i = 0, 1, \ldots, N$. This completes the proof. □

Lemma 3 (Monotonic Source Term case)**.** If $P_i \geq 0$ is nondecreasing with i and also if $k_{i,i} - k_{i,i-1} - k_{i,i+1} \geq \alpha > 0$, then we have another bound

$$|w_i| \leq \max\{|A_1|,\ |A_2|\} + \frac{P_i}{\alpha}, \tag{3.15}$$

so, in this case, the solution's size is affected predictably by the boundary value and the growing source function P_i.

Proof. Let us define the mesh $\Psi_i = \max\{|A_1|,\ |A_2|\} + \frac{1}{\alpha}P_i \pm w_i$. For the boundary points $i = 0$ and $i = N$, we have:

$$\Psi_0 = \max\{|A_1|,\ |A_2|\} + \frac{1}{\alpha}P_0 \pm w_0 \geq 0,$$

$$\Psi_N = \max\{|A_1|,\ |A_2|\} + \frac{1}{\alpha}P_N \pm w_N \geq 0.$$

Now, we apply the difference operator for $1 \leq i \leq N-1$:

$$\begin{aligned}
\mathcal{L}_\langle \Psi_i &= k_{i,i-1}\Psi_{i-1} - k_{i,i}\Psi_i + k_{i,i+1}\Psi_{i+1} \\
&= (k_{i,i-1} - k_{i,i} + k_{i,i+1}) \max\{|A_1|,\ |A_2|\} + \frac{1}{\alpha}\left(k_{i,i-1}P_{i-1} - k_{i,i}P_i + k_{i,i+1}P_{i+1}\right) \pm \mathcal{L}_\langle w_i \\
&= (k_{i,i-1} - k_{i,i} + k_{i,i+1}) \max\{|A_1|,\ |A_2|\} + \frac{1}{\alpha}\left(k_{i,i-1}P_{i-1} - k_{i,i}P_i + k_{i,i+1}P_{i+1}\right) \pm P_i.
\end{aligned}$$

Since P_i is nondecreasing, we know $P_{i-1} \leq P_i \leq P_{i+1}$. Therefore

$$k_{i,i-1}P_{i-1} - k_{i,i}P_i + k_{i,i+1}P_{i+1} \leq (k_{i,i-1} - k_{i,i} + k_{i,i+1})P_i.$$

Thus, $L\Psi_i \geq (k_{i,i-1} - k_{i,i} + k_{i,i+1}) \max\{|A_1|,\ |A_2|\} + \frac{1}{\alpha}(k_{i,i-1} - k_{i,i} + k_{i,i+1})P_i \pm P_i$. Using the assumption $k_{i,i-1} - k_{i,i} + k_{i,i+1} \geq \alpha > 0$, we obtain $\mathcal{L}_\langle \Psi_i \geq 0$. By the discrete maximum principle Lemma 2, we have $\Psi_i \geq 0$, which implies $\pm w_i \leq \max\{|A_1|,\ |A_2|\} + \frac{1}{\alpha}P_i$, and hence $|w_i| \leq \max\{|A_1|,\ |A_2|\} + \alpha^{-1}P_i$. □

The uniqueness of the discrete solution is ensured by the discrete maximum principle. Since the discrete system is linear, the existence of a solution follows from its uniqueness. Moreover, the discrete maximum principle also allows us to establish the boundedness of the numerical solution [26].

Lemma 4 (Uniform stability bound)**.** Assume the reaction coefficient satisfies $d_i \geq \beta_0 > 0$ for all $i = 1, 2, \ldots, N-1$, where β_0 is a uniform positive lower bound independent of ε and h. Then, the solution of the discrete problem

$$\mathcal{L}_h w_i = P_i, \quad i = 1, \ldots, N-1,$$

with boundary conditions $w_0 = A_1$ and $w_N = A_2$, satisfies the uniform bound

$$\|w\|_\infty \leq \max\{|A_1|, |A_2|\} + \frac{1}{\beta_0} \max_{1 \leq i \leq N-1} |P_i|. \tag{3.16}$$

Proof. Define the barrier function $\Psi_i = M \pm w_i$, where $M := \max\{|A_1|, |A_2|\} + \frac{1}{\beta_0}\max_{1 \leq j \leq N-1}|P_j|$. At the boundaries $i = 0$ and $i = N$:

$$\Psi_0 = M \pm w_0 = M \pm A_1 \geq M - |A_1| \geq 0, \quad \Psi_N = M \pm w_N = M \pm A_2 \geq M - |A_2| \geq 0.$$

Interior points ($1 \le i \le N-1$). Using the discrete operator defined in (3.11):

$$\mathcal{L}_h w_i = k_{i,i-1} w_{i-1} - k_{i,i} w_i + k_{i,i+1} w_{i+1},$$

with coefficients $k_{i,i-1} = \frac{\sigma\varepsilon}{h^2} - \frac{c_i}{2h}, \quad k_{i,i} = \frac{2\sigma\varepsilon}{h^2} + d_i, \quad k_{i,i+1} = \frac{\sigma\varepsilon}{h^2} + \frac{c_i}{2h}$, we compute

$$\begin{aligned}\mathcal{L}_h \Psi_i &= k_{i,i-1}(M \pm w_{i-1}) - k_{i,i}(M \pm w_i) + k_{i,i+1}(M \pm w_{i+1}) \\ &= (k_{i,i-1} - k_{i,i} + k_{i,i+1})M \pm (k_{i,i-1} w_{i-1} - k_{i,i} w_i + k_{i,i+1} w_{i+1}) = -d_i M \pm P_i,\end{aligned}$$

where we used the identity $k_{i,i-1} - k_{i,i} + k_{i,i+1} = -d_i$, which follows directly from the coefficient definitions. Since $d_i \ge \beta_0 > 0$ and $M \ge \beta_0^{-1} \max_{1 \le j \le N-1} |P_j|$, we obtain

$$\mathcal{L}_h \Psi_i \le -\beta_0 \cdot \frac{1}{\beta_0} \max_{1 \le j \le N-1} |P_j| + |P_i| \le 0.$$

By Lemma 2, since $\mathcal{L}_h \Psi_i \le 0$ for all interior nodes and $\Psi_i \ge 0$ at the boundaries, we conclude that $\Psi_i \ge 0$ for all $i = 0, 1, \ldots, N$. From $\Psi_i = M \pm w_i \ge 0$ it follows that $-M \le w_i \le M$ for all i, which implies

$$\|w\|_\infty = \max_{0 \le i \le N} |w_i| \le M = \max\{|A_1|, |A_2|\} + \frac{1}{\beta_0} \max_{1 \le i \le N-1} |P_i|.$$

This establishes the uniform bound (3.16). □

Lemma 5. Let $\mathcal{L}_\langle w_i$ be the difference operator defined in equation (3.11). Then, the discrete scheme given in (3.1) becomes:

$$|\mathcal{L}_\langle w_i| \le \|f\|_\infty + C\lambda h \left(A_1 + A_2 + 2 \sum_{j=1}^{i} |w_j| \right), \quad 1 \le i \le N-1 \tag{3.17}$$

Proof. From (3.1), we rewrite $\mathcal{L}_\langle w_i$ as:

$$\mathcal{L}_\langle w_i = f_i - \frac{\lambda h}{2} \left(Z(t_i, t_0) w_0 + 2 \sum_{j=1}^{i-1} Z(t_i, t_j) w_j + Z(t_i, t_i) w_i \right).$$

Taking absolute values,

$$|\mathcal{L}_\langle w_i| \le |f_i| + \left| \frac{\lambda h}{2} Z(i_i, i_0) w_0 \right| + \left| \lambda h \sum_{j=1}^{i-1} Z(t_i, t_j) w_j \right| + \left| \frac{\lambda h}{2} Z(t_i, t_i) w_i \right|$$

Now, assuming $Z(t, x)$ is bounded , say $|Z(t, x)| \le M$, and defining $\|w\|_\infty = \max_j |w_j|$, we get

$$|\mathcal{L}_\langle w_i| \le \|f\|_\infty + \frac{\lambda h}{2} M |w_0| + h\lambda M \sum_{j=1}^{i-1} |w_j| + \frac{\lambda h}{2} M |w_i|$$

Grouping terms

$$|\mathcal{L}_\langle w_i| \le \|f\|_\infty + M\lambda h \left(\frac{1}{2} |w_0| + \sum_{j=1}^{i-1} |w_j| + \frac{1}{2} |w_i| \right)$$

we get $|\mathcal{L}_\langle w_i| \le \|f\|_\infty + C\lambda h (A_1 + A_2 + 2 \sum_{j=1}^{i} |w_j|)$, for $1 \le i \le N-1$. Hence, it is proved. □

Lemma 6. For solution w_i of the difference scheme described in (3.1), the following bound holds:

$$|w_i| \leq \left(\frac{\|f\|_\infty}{\alpha} + \max\{|A_1|,\ |A_2|\} + \frac{Ch\lambda(A_1 + A_2)}{\alpha}\right)\exp\left(\frac{C_1 t_i}{\alpha}\right). \tag{3.18}$$

Proof. Let the scheme

$$\sigma\varepsilon\frac{w_{i+1} - 2w_i + w_{i-1}}{h^2} + c_i\frac{w_{i+1} - w_{i-1}}{2h} - d_i w_i = F$$

where $F = f_i - \frac{\lambda h}{2}\left(Z(t_i, t_0)w_0 + 2\sum_{j=1}^{i-1} Z(t_i, t_j)w_j + Z(t_i, t_i)w_i\right)$, with $w_0 = A_1, \quad and \quad w_N = A_2$ defines $v_i = \lambda h(A_1 + A_2 + 2\sum_{j=1}^{i-1}|w_j|)$ and $C = \frac{M}{2}$ from (3.17). We obtain

$$|\mathcal{L}_\langle w_i| = |F| \leq Cv_i + \|f\|_\infty.$$

By boundedness of solution we have (3.16), so

$$|w_i|_\infty \leq \max\{|A_1|,\ |A_2|\} + \alpha^{-1}(Cv_i + \|f\|_\infty) \leq m + \frac{C_1}{\alpha}\sum_{j=1}^{i-1}|w_j| \tag{3.19}$$

where $m = \max\{|A_1|,\ |A_2|\} + \frac{\|f\|_\infty}{\alpha} + \frac{Ch\lambda(A_1+A_2)}{\alpha}$ and $C_1 = 2Ch\lambda$ using Gronwall's inequality to (3.19) $|w_i| \leq m\exp(\frac{C_1 t_i}{\alpha})$. This shows that

$$|w_i| \leq \left(\frac{\|f\|_\infty}{\alpha} + \max\{|A_1|,\ |A_2|\} + \frac{Ch\lambda(A_1 + A_2)}{\alpha}\right)\exp\left(\frac{C_1 t_i}{\alpha}\right). \tag{3.20}$$

□

3.3.2. Uniform convergence analysis

In this part, we will look into how accurately the method we discussed earlier approximates the true solution. To do that, first define the error at each mesh point t_i as $y_i = W_i - w_i$, where W_i is the numerical solution obtained from the discrete scheme (3.1) and w_i is the exact solution of the original problem (1.2) evaluated at t_i.

This error term y_i, evaluated for $i = 0, 1, ...N$, follows its own discrete relation. By studying this relation, we can gain insights into how the numerical error is distributed and how it evolves throughout the domain.

$$\mathcal{L}_\langle y_i = R_i. \tag{3.21}$$

$$y_0 = 0, \quad y_N = 0 \tag{3.22}$$

Theorem 1. Let $c, f \in C^2[0, 1], Z \in C^2([0, 1] \times [0, 1])$. Then, the remainder term R_i arising from the numerical scheme satisfies the bound:

$$\|R_i\|_\infty \leq Ch^n, \quad n = 1, 2 \tag{3.23}$$

where C is a constant independent of the mesh size h and ε. The error is $O(h)$ when $\varepsilon \ll h$, and $O(h^2)$ when $h \leq \varepsilon$.

Proof. The truncation error of

$$\begin{aligned}\mathcal{L}_\langle(w(t_i)-w_i) = (\mathcal{L}-\mathcal{L}_\langle)w_i &= \left(\varepsilon w_i'' + c(t_i)w_i' - d(t_i)w_i\right) - f(t_i) - \lambda\int_0^t Z(t_i,x)w(x)dx \\ &\quad - \left(\varepsilon\sigma D^+D^-w_i + c_iD^0w_i - d_iw_i - f_i - \lambda\int_0^t Z(t_i,x)w(x)dx\right) \\ &= \left(\varepsilon w_i'' + c(t_i)w_i'\right) - \left(\varepsilon\sigma D^+D^- + c_iD^0w_i\right) + R_1 = R_1 + R_2,\end{aligned}$$

where $R_2 = \varepsilon\left(\frac{d^2}{dt^2} - \sigma D^+D^-\right)w(t_i) + c_i\left(\frac{d}{dt} - D^0\right)w(t_i)$, which satisfies the bound

$$R_2 \le \left|\varepsilon\left[\frac{\rho c(t_i)}{2}\coth\left(\frac{\rho c(t_i)}{2}\right) - 1\right]D^+D^-w(t_i)\right| + \left|\varepsilon\left(\frac{d^2}{dt^2} - D^+D^-w(t_i)\right)\right| + \left|c(t)\left(\frac{d}{dt} - D^0\right)w(t_i)\right| \quad (3.24)$$

with $\rho = \frac{h}{\varepsilon}$ and $\sigma = \frac{\rho c(t)}{2}\coth\left(\frac{\rho c(t)}{2}\right)$. For two constants c_1 and c_2, we have

$$|\rho\coth(\rho) - 1| \le c_1\rho^2, \quad \text{for } \rho \le 1.$$

Since $\coth(\frac{h}{\varepsilon}) \to 1$ as $\frac{h}{\varepsilon} \to 0$, and $\frac{h}{\varepsilon}\coth(\frac{h}{\varepsilon}) \to 1$ as $\frac{h}{\varepsilon} \to \infty$, we have $\left|\frac{h}{\varepsilon}\coth(\frac{h}{\varepsilon}) - 1\right| \le c_2\rho^2$, for all $\rho \ge 0$. Hence, we can write for all $\rho \ge 0$,

$$c_1\frac{\rho^2}{\rho+1} \le \rho\coth(\rho) - 1 \le c_2\frac{\rho^2}{\rho+1}. \quad (3.25)$$

Using (2.12), we can write

$$\varepsilon\left(\frac{c(t)\rho}{2}\coth\left(\frac{c(t)\rho}{2}\right) - 1\right) \le \varepsilon\frac{\rho^2}{\rho+1} = \frac{\hat{h}^2}{h+\varepsilon}. \quad (3.26)$$

Using the Taylor series expansion, we have the bounds

$$\begin{aligned}&\left|D^+D^-w(t_i)\right| \le C\|w'(\zeta)\|, \quad \left|\left(\frac{d}{dt} - D^0\right)w(t_i)\right| \le Ch^2\|w'(\zeta)\|, \\ &\left|\left(\frac{d^2}{dt^2} - D^+D^-\right)w(t_i)\right| \le Ch^2\|w^{(4)}(\zeta)\|, \text{ for } \zeta \in (t_0, t_N).\end{aligned} \quad (3.27)$$

Using (3.27) and (3.26), the truncation error (3.24) becomes

$$R_2 \le \left(\frac{Ch^2}{h+\varepsilon}\right)\|w'(\zeta)\| + \varepsilon Ch^2\|w^{(4)}(\zeta)\| + Ch^2\|w'(\zeta)\|. \quad (3.28)$$

Since the remainder term is $R = R_1 + R_2$. From $R_1 \approx -\frac{h^2}{12}\left[f''(\zeta)\right]$, $f''(x) = \frac{d^2}{dx^2}\left[Z(t_i,x)w(x)\right]$ and from (3.28) we have

$$|R| \le \left|-\frac{h^2}{12}\left[f''(\zeta)\right]\right| + \left(\frac{Ch^2}{h+\varepsilon}\right)\|w'(\zeta)\| + \varepsilon Ch^2\|w^{(4)}(\zeta)\| + Ch^2\|w'(\zeta)\|.$$

Simplifying the above expression, we get $\|R\|_\infty \le \frac{h^2}{12}\|f''\|_\infty + Ch^2\left(\frac{1}{h+\varepsilon} + 1\right)\|w'\|_\infty + \varepsilon Ch^2\|w^{(4)}\|_\infty$

- Term 1: $\frac{h^2}{12}\|f''\|_\infty = O(h^2)$.
- Term 2: $Ch^2\left(\frac{1}{h+\varepsilon}+1\right) \sim \begin{cases} O(h), & \varepsilon \ll h \\ O(h^2), & h \le \varepsilon. \end{cases}$
- Term 3: $\varepsilon Ch^2\|w^{(4)}\|_\infty = O(\varepsilon h^2)$.

Overall, the error is $O(h)$ when $\varepsilon \ll h$, and $O(h^2)$ when $h \le \varepsilon$.

□

Lemma 7. Under the condition that the difference scheme in (3.1) satisfies the discrete maximum principle and is stable, then the solution z_i of the problem $\mathcal{L}_\langle z_i = P_i,\ i = 1, 2, \ldots, N-1,\ \ z_0 = z_N = 0$ satisfies the estimate

$$\|z\|_\infty \le C_3 \max_{1\le i\le N-1} |P_i|.$$

Proof. Given the estimate from (3.18), we have $|z_i| \le \left(\frac{\|f\|_\infty}{\alpha} + \max\{|A_1|,\ |A_2|\} + \frac{Ch\lambda(A_1+A_2)}{\alpha}\right)\exp\left(\frac{C_1 t_i}{\alpha}\right)$, set as $z_0 = A_1 = 0$, $z_N = A_2 = 0$. Then, the estimate becomes $|z_i| \le \alpha^{-1}\|f\|_\infty \exp(\alpha^{-1}C_1 t_i)$.
Let $f_i = P_i$. Then, $|z_i| \le \alpha^{-1}\|R\|_\infty \exp(\alpha^{-1}C_1 t_i)$. Since $t_i \in [0, 1]$, we have $\exp(\alpha^{-1}C_1 t_i) \le \exp(\alpha^{-1}C_1) =: C_2$. Therefore, $|z_i| \le \alpha^{-1}C_2\|R\|_\infty =: C_3 \max_{1\le i\le N-1}|R_i|$. Hence,

$$\|z\|_\infty = \max_{0\le i\le N} |z_i| \le C_3 \max_{1\le i\le N-1} |R_i|.$$

□

Theorem 2. Assume Theorem 1 holds. If the difference scheme in (3.1) or (3.9) is applied to the continuous problem (1.2) or (1.3) on a uniform mesh, then it is uniformly convergent. That is,

$$\|\mathbf{W} - \mathbf{w}\|_\infty \le Ch, \tag{3.29}$$

where $\mathbf{W} = (w_1, \ldots, w_{N-1})^\top$ denotes the numerical solution and $\mathbf{w} = (w(t_1), \ldots, w(t_{N-1}))^\top$ the exact solution sampled at the interior mesh points.

Remark 2. Results of Theorems 1 and 2 illustrate the typical asymptotic error behavior of the exponentially fitted method for the problems in (1.2) or (1.3).

- When the perturbation parameter satisfies $\varepsilon \ge h$, the solution is smooth on the scale of the mesh, and the scheme often exhibits second-order convergence in h (i.e., $O(h^2)$) in practice, due to the high accuracy of the trapezoidal rule and the smoothness of the regular component.
- When $\varepsilon \ll h$, the boundary layer is unresolved by the uniform mesh, and the discretization error saturates at $O(h)$, reflecting the dominant contribution from the layer region.

Consequently, while the method is not uniformly second-order convergent, it is uniformly convergent of first order in the maximum norm across all values of $\varepsilon \in (0, 1]$. This robustness maintaining accuracy without requiring layer adapted meshes is a key advantage of exponentially fitted methods.

4. Numerical results and discussion

In this section, we explore how well the scheme performs by working through a couple of examples that illustrate its stability and accuracy. To evaluate the method, we use two key indicators: the maximum absolute error e_N and the observed convergence rate r_k.

Because the exact solutions are known for the first three examples, we can directly compute the maximum absolute error across all mesh points using the formula

$$e_N = \max_{0\le j\le 1} |w(t_j) - W_j|, \tag{4.1}$$

where $w(t_j)$ is the exact solution and W_j is the approximated solution.

To get a sense of how the accuracy improves with mesh refinement, we calculate the convergence rate with the expression

$$r_k := \log_2\left(\frac{e_{N_k}}{e_{2N_k}}\right), \quad k = 1, 2, 3, \ldots \tag{4.2}$$

This rate helps us understand how quickly the error decreases as we increase the number of mesh points.

Example 1. From [20], we take the following convection dominated VIDE problem

$$\varepsilon w''(t) + w'(t) - w(t) - \int_0^t tw(x)\,dx = -e^{-t/\varepsilon}(1 - \varepsilon t) - \varepsilon t,\ t \in (0, 1),$$

with the boundary conditions $w(0) = 1,\ w(1) = e^{-1/\varepsilon}$. The exact solution is given by: $w(t) = e^{-t/\varepsilon}$.

Example 2. Consider the following convection dominated VIDE problem

$$\varepsilon w''(t) + (1 + t)\,w'(t) + (2 - t)\,w(t) - \int_0^t t\,w(x)\,dx = \left(\frac{-t}{\varepsilon} + 2 - t\right)e^{-t/\varepsilon} - t\varepsilon\left(1 - e^{-t/\varepsilon}\right),\ t \in (0, 1),$$

with the boundary conditions $w(0) = 1,\ \ w(1) = e^{-1/\varepsilon}$, and the exact solution is given by $w(t) = e^{-t/\varepsilon}$.

Example 3. Consider the following convection dominated VIDE problem

$$\varepsilon w''(t) + (2 + 5t^2)w'(t) + (1 + t)w(t) - \int_0^t t^2 w(x)\,dx = f(t),\ t \in (0, 1),$$

with the boundary conditions $w(0) = 1,\ w(1) = 0$. The exact solution is given by $w(t) = (1 - t)e^{-t/\varepsilon}$ for $f(t) = \left(1 - 6x^2 - \frac{(1-t)(1+5t^2)}{\varepsilon} + t^2(\varepsilon - \varepsilon^2) - \varepsilon t^3\right)e^{-t/\varepsilon} - t^2(\varepsilon - \varepsilon^2)$.

Example 4. From [20], we take the nonlinear convection dominated VIDE problem with smooth kernel

$$\varepsilon w''(t) + (1 + t^2)w'(t) = \int_0^t e^{x+w(x)}\,dx + \varepsilon t,\ t \in (0, 1),$$

with boundary conditions $w(0) = 0, \quad w(1) = 0$. The kernel $Z(t, x, w) = e^{x+w}$ is smooth and strictly increasing in w.

For the nonlinear case to approximate the Volterra integral with the composite trapezoidal rule:

$$\int_0^{t_i} e^{x+w(x)}\,dx \approx h\left(\tfrac{1}{2}e^{t_0+w_0} + \sum_{j=1}^{i-1} e^{t_j+w_j} + \tfrac{1}{2}e^{t_i+w_i}\right) =: \mathcal{I}_i(\mathbf{w}),$$

The nonlinear residual vector $\mathbf{R}(\mathbf{u}) \in \mathbb{R}^{N-1}$ for the interior nodes $i = 1, \ldots, N-1$ by

$$R_i(\mathbf{w}) := \varepsilon\frac{w_{i+1} - 2w_i + w_{i-1}}{h^2} + (1 + t_i^2)\frac{w_{i+1} - w_{i-1}}{2h} - \mathcal{I}_i(\mathbf{w}) - \varepsilon t_i.$$

The discrete problem is to find $\mathbf{u} \in \mathbb{R}^{N+1}$ with $w_0 = w_N = 0$ such that $\mathbf{R}(\mathbf{w}) = \mathbf{0}$.

To solve this nonlinear system, we apply Newton's method. Given an initial guess $\mathbf{w}^{(0)} = \mathbf{0}$, the k-th Newton iterate $\mathbf{w}^{(k+1)}$ is obtained by solving the linear system

$$\mathbf{w}^{(k+1)} = \mathbf{w}^{(k)} - \mathbf{J}^{-1}(\mathbf{w}^{(k)})\mathbf{R}(\mathbf{w}^{(k)}),$$

for $k = 0, 1, 2, \ldots$, where $\mathbf{J}(\mathbf{w}) = \partial\mathbf{R}/\partial\mathbf{w}$ is the Jacobian matrix. The Jacobian entries are computed as follows. For $i = 1, \ldots, N-1$:

$$\frac{\partial R_i}{\partial w_{i-1}} = \frac{\varepsilon}{h^2} - \frac{1 + t_i^2}{2h},\ \frac{\partial R_i}{\partial w_i} = -\frac{2\varepsilon}{h^2} - h \cdot \frac{1}{2}e^{t_i+w_i^{(k)}},\ \frac{\partial R_i}{\partial w_{i+1}} = \frac{\varepsilon}{h^2} + \frac{1 + t_i^2}{2h},$$

and for $j = 1, \ldots, i-1$,

$$\frac{\partial R_i}{\partial w_j} = -h\, e^{t_j+w_j^{(k)}}.$$

Note that $\partial R_i/\partial w_j = 0$ for $j > i$, reflecting the causal (lower-triangular) structure of the Volterra operator. Thus, at each Newton step, we solve a sparse, lower-Hessenberg linear system. The iteration is terminated when

$$\|\mathbf{R}(\mathbf{w}^{(k)})\|_\infty < \epsilon = 10^{-5},$$

or when the number of iterations (`MaxIter` = 50) is reached. This Newton linearization ensures quadratic convergence near the solution and robust handling of the nonlinearity induced by the exponential kernel. Since the exact solution is not known, we used the double mesh technique for calculating the maximum absolute error of this example.

To validate the effectiveness of the proposed method, numerical experiments are conducted using four examples. The first three examples are linear and the fourth example is nonlinear. The objective was to analyze the ability of the method in terms of producing accurate results and maintain uniform convergence under varying mesh sizes and perturbation parameters ε. Figure 1 (a) displays numerical solutions of Examples 1 for different values of perturbation parameter ε, and in Figure 1 (b) the absolute error of the methods for different ε are depicted. As we observe in Figure 1 (a) when the values of ε decrease, a sharp boundary layer formed near the left boundary, specifically around $x = 0$, and become more pronounced with smaller ε values. Beyond this region, the solution remains smooth and nearly flat throughout the rest of the domain. These figures demonstrate that the proposed method accurately captures the steep gradients within this layer region, effectively addressing one of the main challenges in solving the considered problems using the classical numerical methods. To further evaluate the method's accuracy, point-wise absolute errors are plotted in Figure 1 (b). As seen in the figure,

as ε decreases, the error increases due to sharper boundary layers but remains uniformly bounded, confirming the method's robustness for fixed N. In Figure 2, similar results of Example 2 are given. Figure 3 shows error trends for fixed ε as N increases. The downward error trajectory supports the method's convergence as N grows.

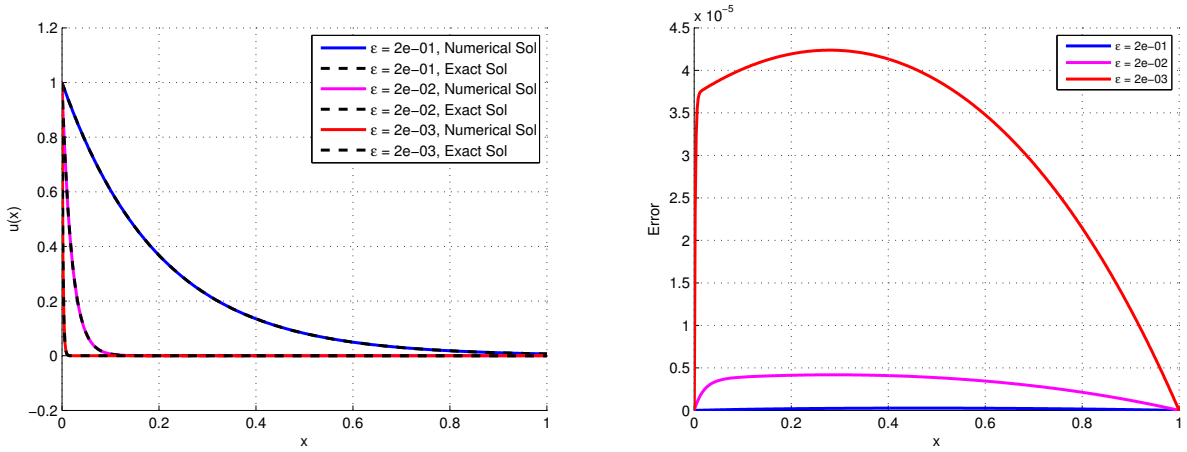

Figure 1. Solution behavior of Example 1 on the left and its point-wise absolute error on the right side with a fixed mesh size of $N = 500$ as ε decreases.

Tables 1, 2, 3 present the point-wise maximum absolute errors for Examples 1, 2, and 3, respectively, under multiple ε values and increasing mesh numbers. These results reveal a consistent decline in error with denser discretization, highlighting the method's mesh sensitivity and reliability. In each of these tables, the maximum point-wise absolute error is bounded as ε decreases from 10^{-2} to 10^{-5}. This guarantees the uniform convergence of the method independent of the parameter ε. Tables 4 and 5 examines convergence rate of the proposed method for Examples 1 and 2. For larger ε, the method achieves nearly second-order convergence. However, as $\varepsilon \to 0$, convergence rates slightly decrease but remain within a satisfactory range (above 1.00 for very small ε), which aligns well with theoretical expectations stated in Remark 2. Tables 6, 7, 8, and 9 provide comparative results between the proposed exponentially fitted method and the method without the fitting parameter σ. These tables show comparison of the maximum point-wise absolute error of the exponentially fitted method and the method without the fitting parameter. As observed from the tables, the exponentially fitted scheme is more accurate and stable for all ε values whereas the unfitted scheme diverges as $\varepsilon \to 0$. These results show the benefit of the fitted method. In Tables 10 and 11, comparison of the rate of convergence of the exponentially fitted method and the unfitted method is given. As one observes, the fitted scheme has an order of convergence one for the case $\varepsilon \ll h$, whereas for the case $\varepsilon \geq h$ it has two, the same as it is discussed in Remark 2. In the unfitted scheme, the rate of convergence goes to zero as ε becomes small, which indicates the instability of the unfitted method for convection dominated VIDEs.

In Table 12, comparison of the maximum absolute error of the proposed method and the hybrid method in [20] is made for Example 1. The results in this table indicate that the two method give equivalent accuracy across different values of ε. In Table 13, comparison of the absolute error and rate of convergence of the proposed method and the hybrid method in [20] and its extrapolated form is made for Example 4. The results in the table show that proposed method gives equivalent accuracy and

rate of convergence with the hybrid scheme in [20], but it gives lower results than the extrapolated form of the method. In Table 14, the computational time of the proposed method and the method in [20] is depicted for Examples 1 and 4. As one observes, the proposed method has smaller computation time compared to the methods in [20]. While post-processing (or extrapolation techniques) in [20] can further reduce errors, it requires multi-grid solution and significantly increases computational cost. The proposed method offers a favorable accuracy-efficiency trade-off for applications prioritizing speed and implementation simplicity.

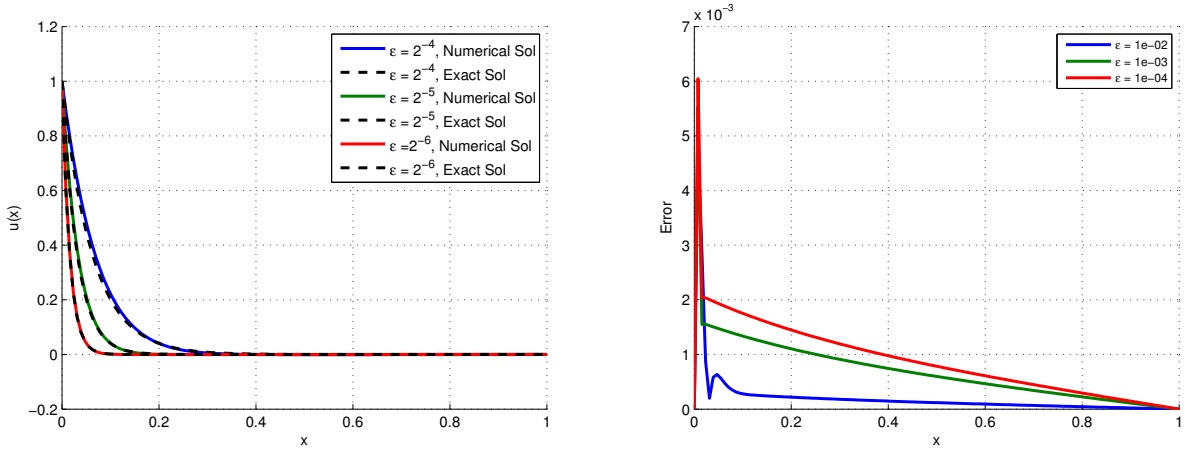

Figure 2. Solution behavior of Example 2 on the left and its point-wise absolute error on the right side with a fixed mesh size of $N = 500$ as ε decreases.

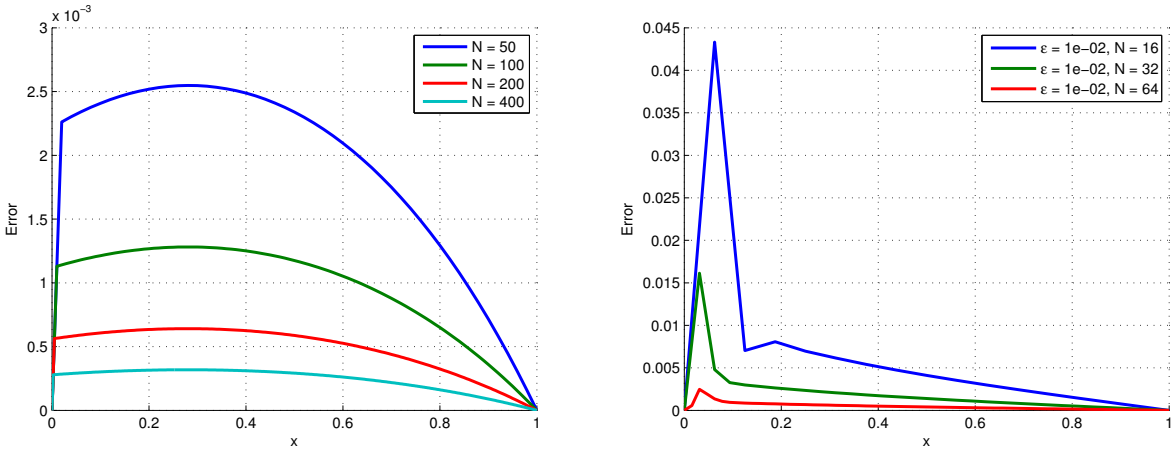

Figure 3. Point-wise absolute error using the proposed method for Example 1 on the left and Example 2 on the right with increasing mesh size N, and fixed $\varepsilon = 2^{-05}$.

Table 1. Maximum absolute error of the proposed method for Example 1.

$\varepsilon \downarrow$	$N = 128$	$N = 256$	$N = 512$	$N = 1024$	$N = 2048$
10^{-2}	1.28E−04	3.24E−05	8.11E−06	2.03E−06	5.07E−07
10^{-3}	7.50E−04	2.67E−04	7.75E−05	2.03E−05	5.12E−06
10^{-4}	9.81E−04	4.79E−04	2.27E−04	1.01E−04	3.83E−05
10^{-5}	1.00E−03	5.02E−04	2.50E−04	1.24E−04	6.07E−05

Table 2. Maximum absolute error of the proposed method for Example 2.

$\varepsilon \downarrow$	$N = 128$	$N = 256$	$N = 512$	$N = 1024$	$N = 2048$
10^{-2}	8.49E-04	2.06E-04	5.10E-05	1.27E-05	3.18E-06
10^{-3}	5.52E-03	2.25E-03	6.29E-04	1.32E-04	3.24E-05
10^{-4}	6.05E-03	2.99E-03	1.47E-03	7.06E-04	3.10E-04
10^{-5}	6.10E-03	3.04E-03	1.52E-03	7.57E-04	3.76E-04

Table 3. Maximum absolute error of the proposed fitted method for Example 3.

N	$\varepsilon = 10^{-2}$	$\varepsilon = 10^{-3}$	$\varepsilon = 10^{-4}$	$\varepsilon = 10^{-5}$
128	1.29E−04	7.52E−04	9.82E−04	1.00E−03
256	3.25E−05	2.68E−04	4.79E−04	5.02E−04
512	8.12E−06	7.76E−05	2.27E−04	2.50E−04
1024	2.03E−06	2.03E−05	1.01E−04	1.24E−04
2048	5.07E−07	5.12E−06	3.83E−05	6.07E−05

Table 4. Convergence rate of the proposed method of Example 1.

$\varepsilon \downarrow$	r_1	r_2	r_3	r_4
10^{-2}	1.99	2.00	2.00	2.00
10^{-3}	1.49	1.79	1.94	1.98
10^{-4}	1.03	1.08	1.17	1.39
10^{-5}	1.00	1.01	1.01	1.03

Table 5. Convergence rate of the proposed method for Example 2.

$\varepsilon \downarrow$	r_1	r_2	r_3	r_4
10^{-2}	2.05	2.01	2.00	2.00
10^{-3}	1.30	1.84	2.25	2.03
10^{-4}	1.01	1.03	1.06	1.19
10^{-5}	1.00	1.00	1.01	1.01

Table 6. Maximum point-wise absolute errors using the proposed method and the unfitted method ($\sigma = 1$) for Example 1.

N	$\varepsilon = 10^{-2}$		$\varepsilon = 10^{-3}$		$\varepsilon = 10^{-4}$		$\varepsilon = 10^{-5}$	
	Unfitted	Fitted	Unfitted	Fitted	Unfitted	Fitted	Unfitted	Fitted
128	1.94E−02	1.28E−04	5.88E−01	7.50E−04	9.43E−01	9.81E−04	1.11E+00	1.00E−03
256	4.62E−03	3.24E−05	3.42E−01	2.67E−04	8.99E−01	4.79E−04	1.00E+00	5.02E−04
512	1.16E−03	8.11E−06	1.30E−01	7.75E−05	8.13E−01	2.27E−04	9.78E−01	2.50E−04
1024	2.88E−04	2.03E−06	3.27E−02	2.03E−05	6.59E−01	1.01E−04	9.59E−01	1.24E−04
2048	7.20E−05	5.07E−07	7.49E−03	5.12E−06	4.26E−01	3.83E−05	9.21E−01	6.07E−05

Table 7. Comparison of maximum point-wise absolute errors using the proposed fitted method and the unfitted method ($\sigma = 1$) for Example 2.

N	$\varepsilon = 10^{-2}$		$\varepsilon = 10^{-3}$		$\varepsilon = 10^{-4}$		$\varepsilon = 10^{-5}$	
	Unfitted	Fitted	Unfitted	Fitted	Unfitted	Fitted	Unfitted	Fitted
128	2.05E−02	8.49E−04	6.04E−01	5.52E−03	1.11E+00	6.05E−03	1.60E+00	6.10E−03
256	4.89E−03	2.06E−04	3.47E−01	2.25E−03	9.10E−01	2.99E−03	2.45E+01	3.04E−03
512	1.22E−03	5.10E−05	1.31E−01	6.29E−04	8.18E−01	1.47E−03	9.93E−01	1.52E−03
1024	3.05E−04	1.27E−05	3.29E−02	1.32E−04	6.62E−01	7.06E−04	9.62E−01	7.57E−04
2048	7.61E−05	3.18E−06	7.54E−03	3.24E−05	4.27E−01	3.10E−04	9.22E−01	3.76E−04

Table 8. Comparison of maximum absolute errors of the proposed fitted method and the unfitted method for Example 3 for different ε.

N	$\varepsilon = 10^{-4}$		$\varepsilon = 10^{-5}$		$\varepsilon = 10^{-6}$	
	Fitted	Unfitted	Fitted	Unfitted	Fitted	Unfitted
256	4.82E−04	9.41E−01	5.03E−04	9.94E−01	5.04E−04	1.00E+00
512	2.29E−04	8.82E−01	2.51E−04	9.78E−01	2.52E−04	9.98E−01
1024	1.02E−04	7.05E−01	1.25E−04	9.57E−01	1.26E−04	9.96E−01
2048	3.87E−05	4.21E−01	6.12E−05	9.15E−01	6.25E−05	9.92E−01
4096	1.50E−05	1.87E−01	3.01E−05	8.32E−01	3.10E−05	9.85E−01

Table 9. Comparison of maximum absolute errors of the proposed fitted method and the unfitted method for the nonlinear Example 4 for different ε.

N	$\varepsilon = 10^{-2}$		$\varepsilon = 10^{-3}$		$\varepsilon = 10^{-4}$		$\varepsilon = 10^{-5}$	
	Fitted	Unfitted	Fitted	Unfitted	Fitted	Unfitted	Fitted	Unfitted
128	1.30E−04	1.95E−02	7.55E−04	5.90E−01	9.85E−04	9.45E−01	1.01E−03	1.12E+00
256	3.26E−05	4.65E−03	2.69E−04	3.45E−01	4.80E−04	9.02E−01	5.03E−04	1.01E+00
512	8.13E−06	1.17E−03	7.77E−05	1.32E−01	2.28E−04	8.15E−01	2.51E−04	9.80E−01
1024	2.03E−06	2.90E−04	2.04E−05	3.30E−02	1.02E−04	6.62E−01	1.25E−04	9.61E−01
2048	5.07E−07	7.25E−05	5.13E−06	7.55E−03	3.85E−05	4.28E−01	6.10E−05	9.23E−01

Table 10. Comparison of convergence rates of the proposed fitted method and unfitted method for Example 3 for different ε.

Rate	$\varepsilon = 10^{-2}$		$\varepsilon = 10^{-3}$		$\varepsilon = 10^{-4}$		$\varepsilon = 10^{-5}$	
	Fitted	Unfitted	Fitted	Unfitted	Fitted	Unfitted	Fitted	Unfitted
r_1	1.99	2.07	1.49	0.78	1.03	0.10	1.00	0.02
r_2	2.00	2.00	1.79	1.39	1.08	0.32	1.01	0.03
r_3	2.00	2.01	1.94	1.99	1.17	0.74	1.01	0.07
r_4	2.00	2.00	1.98	2.13	1.39	1.17	1.03	0.14

Table 11. Comparison of convergence rates of the proposed fitted method and the unfitted method for the nonlinear Example 4 for different ε.

Rate	$\varepsilon = 10^{-2}$		$\varepsilon = 10^{-3}$		$\varepsilon = 10^{-4}$		$\varepsilon = 10^{-5}$	
	Fitted	Unfitted	Fitted	Unfitted	Fitted	Unfitted	Fitted	Unfitted
r_1	1.99	2.07	1.49	0.77	1.03	0.07	1.00	0.01
r_2	2.00	2.00	1.79	1.38	1.08	0.32	1.01	0.02
r_3	2.00	2.01	1.93	2.00	1.16	0.74	1.01	0.06
r_4	2.00	2.00	1.99	2.13	1.40	1.17	1.03	0.14

Table 12. Comparison of the point-wise maximum absolute errors of the Hybrid scheme in [20] before extrapolation and the proposed method for Example 1.

N	$\varepsilon = 10^{-2}$		$\varepsilon = 10^{-3}$		$\varepsilon = 10^{-5}$	
	Hybrid in [20]	Proposed	Hybrid in [20]	Proposed	Hybrid in [20]	Proposed
128	2.90E−3	1.28E−4	2.85E−3	7.50E−4	2.83E−3	1.00E−3
256	9.54E−4	3.24E−5	9.32E−4	2.67E−4	9.22E−4	5.02E−4
512	3.05E−4	8.11E−6	2.95E−4	7.75E−5	2.91E−4	2.50E−4
1024	9.71E−5	2.03E−6	9.14E−5	2.03E−5	8.99E−5	1.24E−4

Table 13. Comparison of the maximum absolute errors and convergence rates of the proposed fitted method and methods in [20] for Example 4.

Proposed method												
N	$\varepsilon = 10^{-1}$		$\varepsilon = 10^{-2}$		$\varepsilon = 10^{-3}$		$\varepsilon = 10^{-4}$		$\varepsilon = 10^{-5}$		$\varepsilon = 10^{-6}$	
	Error	Rate	Error	Rate	Error	Rate	Error	Rate	Error	Rate	Error	Rate
32	1.30E−03	—	2.10E−03	—	1.80E−03	—	1.80E−03	—	1.80E−03	—	1.80E−03	—
64	3.20E−04	2.02	5.20E−04	2.01	9.00E−04	1.00	9.00E−04	1.00	9.00E−04	1.00	9.00E−04	1.00
128	8.00E−05	2.00	1.30E−04	2.00	7.60E−04	1.24	9.90E−04	1.14	9.90E−04	1.04	9.90E−04	1.04
256	2.00E−05	2.00	3.30E−05	1.98	2.70E−04	1.49	4.80E−04	1.04	4.80E−04	1.04	4.80E−04	1.04
512	5.00E−06	2.00	8.10E−06	2.03	7.80E−05	1.79	2.30E−04	1.06	2.30E−04	1.06	2.30E−04	1.06
1024	1.30E−06	1.94	2.00E−06	2.02	2.00E−05	1.96	1.00E−04	1.20	1.00E−04	1.20	1.00E−04	1.20
Hybrid method in [20] before extrapolation												
N	$\varepsilon = 10^{-1}$		$\varepsilon = 10^{-2}$		$\varepsilon = 10^{-3}$		$\varepsilon = 10^{-4}$		$\varepsilon = 10^{-5}$		$\varepsilon = 10^{-6}$	
	Error	Rate	Error	Rate	Error	Rate	Error	Rate	Error	Rate	Error	Rate
32	7.82E−03	—	9.37E−03	—	9.59E−03	—	9.61E−03	—	9.61E−03	—	9.61E−03	—
64	4.15E−03	0.92	5.42E−03	0.79	5.54E−03	0.79	5.55E−03	0.79	5.55E−03	0.79	5.55E−03	0.79
128	2.14E−03	0.96	3.11E−03	0.80	3.17E−03	0.81	3.17E−03	0.81	3.17E−03	0.81	3.17E−03	0.81
256	1.09E−03	0.98	1.75E−03	0.83	1.78E−03	0.83	1.78E−03	0.83	1.78E−03	0.83	1.78E−03	0.83
512	5.48E−04	0.99	9.66E−04	0.85	9.82E−04	0.86	9.84E−04	0.86	9.84E−04	0.86	9.84E−04	0.86
1024	2.75E−04	0.99	5.27E−04	0.87	5.36E−04	0.87	5.37E−04	0.87	5.37E−04	0.87	5.37E−04	0.87
Hybrid method in [20] after extrapolation												
N	$\varepsilon = 10^{-1}$		$\varepsilon = 10^{-2}$		$\varepsilon = 10^{-3}$		$\varepsilon = 10^{-4}$		$\varepsilon = 10^{-5}$		$\varepsilon = 10^{-6}$	
	Error	Rate	Error	Rate	Error	Rate	Error	Rate	Error	Rate	Error	Rate
32	6.03E−04	—	9.19E−04	—	9.28E−04	—	9.23E−04	—	9.23E−04	—	9.23E−04	—
64	1.71E−04	1.82	3.61E−04	1.35	3.65E−04	1.34	3.64E−04	1.34	3.63E−04	1.34	3.63E−04	1.34
128	4.55E−05	1.91	1.31E−04	1.47	1.32E−04	1.47	1.32E−04	1.47	1.32E−04	1.47	1.32E−04	1.47
256	1.18E−05	1.95	4.42E−05	1.56	4.47E−05	1.57	4.46E−05	1.56	4.45E−05	1.56	4.45E−05	1.56
512	3.00E−06	1.98	1.42E−05	1.64	1.44E−05	1.64	1.44E−05	1.63	1.43E−05	1.64	1.43E−05	1.64
1024	7.55E−07	1.99	4.41E−06	1.69	4.46E−06	1.69	4.43E−06	1.70	4.45E−06	1.69	4.45E−06	1.69

Table 14. Comparison of central processing unit (CPU) time (in seconds) for Example 1.

ε	Proposed Method				Methods in [20]	
	N=128	N=256	N=512	N=1024	Hybrid Method	Extrapolated Method
Example 1						
10^{-2}	0.004	0.019	0.036	0.142	1.822	7.613
10^{-3}	0.004	0.009	0.036	0.141	1.769	9.058
10^{-5}	0.004	0.009	0.036	0.146	1.988	7.686
10^{-7}	0.005	0.009	0.037	0.142	1.687	8.157
Example 4						
10^{-2}	0.142	0.580	2.350	9.870	7.475	18.838
10^{-3}	0.138	0.550	2.280	9.450	7.224	19.286
10^{-5}	0.151	0.610	2.470	10.120	7.213	19.586
10^{-7}	0.149	0.590	2.410	9.980	7.613	19.331

5. Conclusions

This paper focuses on solving linear and nonlinear convection dominated VIDEs. The considered problem exhibits boundary layers on the left side of the domain that cause multiscale nature on the solution. The standard numerical methods fail to solve the problem accurately. We designed an

exponentially fitted difference method for treating the considered linear and nonlinear convection dominated VIDEs. The differential part of the equation is approximated using an exponentially fitted difference method. For the integral part, the composite Trapezoidal rule is applied on uniform mesh. For the nonlinear case, Newton linearization is applied for simplifying the problem. Stability and convergence of the proposed method are analyzed, and how the perturbation parameter influences the solution profile is discussed. The analysis demonstrates that the proposed method achieves uniform convergence with first-order convergence. To support this, four numerical examples are presented with linear and nonlinear form, confirming the stability and reliability of the method. The results confirm that the exponentially fitted difference method is accurate and effectively addresses the numerical challenges posed by the perturbation parameter. The method delivers stable solutions even for small perturbation parameters and maintains consistent performance across varying mesh resolutions. This establishes the method as a reliable and practical tool for solving a broad class of singularly perturbed integro-differential problems. In future, we will consider extensions to systems of convection dominated VIDEs, developing higher-order schemes, and time-dependent form of the considered problem.

Use of Generative-AI tools declaration

The authors declare they have not used Artificial Intelligence (AI) tools in the creation of this article.

Author contributions

Y.A.W conceptualization, Formal analysis and Methodology; M.A. Conceptualization and Validation; M.A. Conceptualization and Validation and Resources M.M.W. Writing review & editing and Writing review & editing

Acknowledgments

The authors thank the reviewers for their valuable comments, which improved the manuscript, and the Deanship of Scientific Research at King Faisal University for their financial support.

This work was supported by the Deanship of Scientific Research, Vice Presidency for Graduate Studies and Scientific Research, King Faisal University, Saudi Arabia [Grant No. KFU263001].

Conflict of interest

The authors declare that there is no any conflict of interest on the publication of the manuscript.

References

1. G. M. Amiraliyev, O. Yapman, M. Kudu, A fitted approximate method for a volterra delay-integro-differential equation with initial layer, *Hacet. J. Math. Stat.*, **48** (2019), 1417–1429.
2. A. M. Bijura, Initial-layer theory and model equations of volterra type, *IMA J. Appl. Math.*, **71** (2006), 315–331.

3. A. Lodge, *Nonlinear Viscoelastic Solids*, Academic Press, 1978.
4. S. Noeiaghdam, M. A. Miah, S. Micula, Homotopy analysis method and physics-informed neural networks for solving volterra integral equations with discontinuous kernels, *Axioms*, **14** (2025), 726. https://doi.org/10.3390/axioms14100726
5. S. Noeiaghdam, D. Sidorov, A. Dreglea, A novel numerical optimality technique to find the optimal results of volterra integral equation of the second kind with discontinuous kernel, *Appl. Numer. Math.*, **186** (2023), 202–212. https://doi.org/10.1016/j.apnum.2023.01.011
6. L. Prandtl, Uber flussigkeitsbewegung bei sehr kleiner reibung, *Verhandl. 3rd Int. Math. Kongr. Heidelberg (1904), Leipzig*.
7. R. Christensen, *Theory of Viscoelasticity: An Introduction*, Academic Press, 1982.
8. S. Noeiaghdam, S. Micula, A novel method for solving second kind volterra integral equations with discontinuous kernel, *Mathematics*, **9** (2021), 2172. https://doi.org/10.3390/math9172172
9. W. Remili, S. Noeiaghdam, Shifted chebyshev collocation with cestac-cadna-based instability detection for nonlinear Volterraa-Hammerstein integral equations, *Math. Comput. Simul.*, **246** (2026), 60–77. https://doi.org/10.1016/j.matcom.2026.01.029
10. M. E. Gurtin, A. C. Pipkin, A general theory of heat conduction with finite wave speeds, *Arch. Ration. Mech. An.*, **31** (1968), 113–126, https://doi.org/10.1007/BF00281373
11. M. Fabrizio, A. Morro, *Mathematical Problems in Linear Viscoelasticity*, SIAM, 1992.
12. J. Cushing, *Periodic Solutions of Nonlinear Integrodifferential Equations in Population Dynamics*, **32** (1994).
13. O. Diekmann, S. van Gils, S. Verduyn Lunel, H. O. Walther, *Delay Equations: Functional-, Complex-, and Nonlinear Analysis*, Springer, 1995.
14. C. BURNAP, M. A. KAZEMI, Optimal control of a system governed by nonlinear volterra integral equations with delay, *IMA J. Math. Control. I.*, **16** (1999), 73–89. https://doi.org/10.1093/imamci/16.1.73
15. N. Krasovskii, *Stability of Motion*, Stanford University Press, 1963.
16. S. i. Amari, Dynamics of pattern formation in lateral-inhibition type neural fields, *Biol. Cybern.*, **27** (1977), 77–87. https://doi.org/10.1007/BF00337259
17. D. Brigo, F. Mercurio, *Interest rate models—Theory and practice: With smile, inflation and credit*, Springer, 2006.
18. P. Markowich, *The Stationary Semiconductor Device Equations*, Springer, 1990.
19. J. S. Angell, W. E. Olmstead, Singularly perturbed volterra integral equations, *SIAM J. Appl. Math.*, **47** (1987), 1–14, https://doi.org/10.1137/0147001
20. A. Panda, J. Mohapatra, On the convergence analysis of efficient numerical schemes for singularly perturbed second order volterra integro-differential equations, *J. Appl. Math. Comput.*, **69** (2023), 3509–3532. https://doi.org/10.1007/s12190-023-01890-8
21. T. A. Burton, *Volterra integral and differential equations*, vol. 202, Elsevier, 2005.

22. A. Panda, J. Mohapatra, I. Amirali, A second-order post-processing technique for singularly perturbed volterra integro-differential equations, *Mediterr. J. Math.*, **18** (2021), 25. https://doi.org/10.1007/s00009-021-01873-8

23. M. M. Woldaregay, G. F. Duressa, Parameter uniform numerical method for singularly perturbed parabolic differential difference equations, *J. Nigerian Math. Soc.*, **38** (2019), 223–245.

24. M. Cakir, B. Gunes, A fitted operator finite difference approximation for singularly perturbed Volterra—Fredholm integro-differential equations, *Mathematics*, **10** (2022), 3560. https://doi.org/10.3390/math10193560

25. M. K. Kadalbajoo, V. Gupta, A brief survey on numerical methods for solving singularly perturbed problems, *Appl. Math. Comput.*, **217** (2010), 3641–3716. https://doi.org/10.1016/j.amc.2010.09.059

26. B. C. Iragi, J. B. Munyakazi, A uniformly convergent numerical method for a singularly perturbed volterra integro-differential equation, *Int. J. Comput. Math.*, **97** (2020), 759–771, https://doi.org/10.1080/00207160.2019.1585828

27. O. Yapman, G. M. Amiraliyev, A novel second-order fitted computational method for a singularly perturbed volterra integro-differential equation, *Int. J. Comput. Math.*, **97** (2020), 1293–1302. https://doi.org/10.1080/00207160.2019.1614565

28. L. B. Liu, L. Ye, X. Bao, Y. Zhang, A second order numerical method for a volterra integro-differential equation with a weakly singular kernel, *Netw. Heterog. Media*, **19** (2024), 740–752. URL `https://doi.org/10.3934/nhm.2024033`

29. J. S. Angell, W. E. Olmstead, Singularly perturbed volterra integral equations ii, *SIAM J. Appl. Math.*, **47** (1987), 1150–1162. https://doi.org/10.1137/0147077

30. J. S. Angell, W. E. Olmstead, Singularly perturbed volterra integral equations ii, *SIAM J. Appl. Math.*, **47** (1987), 1150–1162. https://doi.org/10.1137/0147077

31. T. Koto, Stability of Runge—Kutta methods for delay integro-differential equations, *J. Comput. Appl. Math.*, **145** (2002), 483–492. https://doi.org/10.1016/S0377-0427(01)00596-9

32. S. Wu, S. Gan, Errors of linear multistep methods for singularly perturbed volterra delay-integro-differential equations, *Math. Comput. Simul.*, **79** (2009), 3148–3159. https://doi.org/10.1016/j.matcom.2009.03.006

33. M. M. Woldaregay, G. F. Duressa, Boundary layer resolving exact difference scheme for solving singularly perturbed convection-diffusion-reaction equation, *Math. Probl. Eng.*, **2022** (2022), 2043323. https://doi.org/10.1155/2022/2043323

34. M. M. Woldaregay, G. F. Duressa, Uniformly convergent numerical scheme for singularly perturbed parabolic pdes with shift parameters, *Math. Probl. Eng.*, **2021** (2021), 6637661. https://doi.org/10.1155/2021/6637661

35. E. Doolan, J. Miller, W. Schilders, *Uniform Numerical Methods for Problems with Initial and Boundary Layers*, Boole Press, 1980.

36. J. Miller, E. O'Riordan, G. Shishkin, *Fitted Numerical Methods for Singular Perturbation Problems*, World Scientific, 1996.

37. A. Salama, D. Evans, Fourth order scheme of exponential type for singularly perturbed volterra integro-differential equations, *Int. J. Comput. Math.*, **77** (2001), 153–164. https://doi.org/10.1080/00207160108805058

38. E. Cimen, S. Yatar, A numerical method for solving linear volterra delay integro-differential equations using fitted difference scheme, *Adv. Differ. Equ-NY.*, **2020** (2020), 1–16. https://doi.org/10.1186/s13662-020-02580-w

39. J. J. H. Miller, E. O'riordan, G. I. Shishkin, *Fitted numerical methods for singular perturbation problems: error estimates in the maximum norm for linear problems in one and two dimensions*, World scientific, 2012.

40. G. F. Duressa, M. M. Woldaregay, Fitted numerical scheme for solving singularly perturbed parabolic delay partial differential equations, *Tamkang J. Math.*, **53** (2022), 345–362. https://doi.org/10.5556/j.tkjm.53.2022.3638

AIMS Press